UCLA

Title

Blocking Genomic Instability Prevents Acquired Resistance to MAPK Inhibitor Therapy in Melanoma

Authors

Dharanipragada, Prashanthi
Zhang, Xiao
Liu, Sixue
et al.

Blocking Genomic Instability Prevents Acquired Resistance to MAPK Inhibitor Therapy in Melanoma

Prashanthi Dharanipragada[1], Xiao Zhang[1], Sixue Liu[1], Shirley H. Lomeli[1], Aayoung Hong[1], Yan Wang[1,2], Zhentao Yang[1], Kara Z. Lo[3], Agustin Vega-Crespo[3], Antoni Ribas[2,3,4,5], Stergios J. Moschos[6,7], Gatien Moriceau[1], and Roger S. Lo[1,2,5]

ABSTRACT

Blocking cancer genomic instability may prevent tumor diversification and escape from therapies. We show that, after MAPK inhibitor (MAPKi) therapy in patients and mice bearing patient-derived xenografts (PDX), acquired resistant genomes of metastatic cutaneous melanoma specifically amplify resistance-driver, nonhomologous end-joining (NHEJ), and homologous recombination repair (HRR) genes via complex genomic rearrangements (CGR) and extrachromosomal DNAs (ecDNA). Almost all sensitive and acquired-resistant genomes harbor pervasive chromothriptic regions with disproportionately high mutational burdens and significant overlaps with ecDNA and CGR spans. Recurrently, somatic mutations within ecDNA and CGR amplicons enrich for HRR signatures, particularly within acquired resistant tumors. Regardless of sensitivity or resistance, breakpoint–junctional sequence analysis suggests NHEJ as critical to double-stranded DNA break repair underlying CGR and ecDNA formation. In human melanoma cell lines and PDXs, NHEJ targeting by a DNA-PK$_{CS}$ inhibitor prevents/delays acquired MAPKi resistance by reducing the size of ecDNAs and CGRs early on combination treatment. Thus, targeting the causes of genomic instability prevents acquired resistance.

SIGNIFICANCE: Acquired resistance often results in heterogeneous, redundant survival mechanisms, which challenge strategies aimed at reversing resistance. Acquired-resistant melanomas recurrently evolve resistance-driving and resistance-specific amplicons via ecDNAs and CGRs, thereby nominating chromothripsis–ecDNA–CGR biogenesis as a resistance-preventive target. Specifically, targeting DNA-PK$_{CS}$/NHEJ prevents resistance by suppressing ecDNA/CGR rearrangements in MAPKi-treated melanomas.

INTRODUCTION

Acquired resistance to targeting of oncogenic pathways is the rule rather than the exception. Genetic mechanisms of acquired resistance across malignancies often occur as focal amplifications of resistance-driver genes. Scientific efforts to reverse the consequences of resistance evolution have focused largely on targeting acquired vulnerabilities. In contrast, relatively little is known regarding the mechanisms—for example, genomic instability pathways—that enable rapid resistance evolution of cancer in patients treated with pathway-targeted therapies. Variable levels of focal gene amplifications can confer phenotypic plasticity, fine-tuning tumor cell fitness in response to the selective pressure of therapies.

BRAF inhibitor (BRAFi) therapy of $BRAF^{V600MUT}$ metastatic cutaneous melanoma targets the MAPK pathway and leads quickly to acquired resistance (1). Genetic mechanisms of acquired BRAFi resistance most often result in reactivation of the MAPK pathway, which can be suppressed by adding a MEK inhibitor (MEKi; refs. 2–5). However, with combined BRAFi and MEKi therapy of patients with $BRAF^{V600MUT}$ melanoma, less than 20% of patients survive past 5 years (6). Acquired resistance to BRAFi + MEKi therapy in patients occurs through high-amplitude gene amplifications that, individually or in combination, can reactivate the MAPK pathway (7–9). Hence, there is a need to understand the origins of such genomic instability. For patients with melanoma driven by $NRAS$ mutations, MAPK inhibitor (MAPKi) therapy is currently not available, as MEKi monotherapy is of limited clinical activity (10). However, agents added to MEKi to suppress acquired MEKi resistance may deliver clinically meaningful efficacy (11). Recent analysis of patient-derived xenografts (PDX) of $NRAS^{MUT}$ melanoma with acquired MEKi resistance points to similar genomic events (i.e., focal amplifications of $BRAF^{WT}$, $CRAF^{WT}$, and $NRAS^{MUT}$ genes) as drivers of acquired resistance (11).

Here, we test the hypothesis that chromothripsis and derivative amplicons of resistance-driver genes confer melanoma with genetic variants necessary to resist MAPKi therapy. Cutaneous melanoma is a cancer in which the chromothripsis burden is already high without prior targeted therapy, and chromothripsis appears to be a key evolutionary mechanism by which cancer rapidly generates and accumulates highly dynamic structural variants (SV; ref. 12). SV-related amplicons

[1]Division of Dermatology, Department of Medicine, David Geffen School of Medicine, University of California, Los Angeles, Los Angeles, California. [2]Department of Molecular and Medical Pharmacology, David Geffen School of Medicine, University of California, Los Angeles, Los Angeles, California. [3]Division of Hematology/Oncology, Department of Medicine, David Geffen School of Medicine, University of California, Los Angeles, Los Angeles, California. [4]Division of Surgical Oncology, Department of Surgery, David Geffen School of Medicine, University of California, Los Angeles, Los Angeles, California. [5]Jonsson Comprehensive Cancer Center, David Geffen School of Medicine, University of California, Los Angeles, Los Angeles, California. [6]Division of Medical Oncology, Department of Medicine, The University of North Carolina at Chapel Hill, Chapel Hill, North Carolina. [7]Lineberger Comprehensive Cancer Center, The University of North Carolina at Chapel Hill, Chapel Hill, North Carolina.

Note: P. Dharanipragada and X. Zhang contributed equally to this article.

G. Moriceau and R.S. Lo share senior authorship of this article.

Corresponding Author: Roger S. Lo, University of California, Los Angeles, 10833 Le Conte Avenue, 52-121 CHS Department of Medicine, Division of Dermatology, Los Angeles, CA 90095-1750. Phone: 310-825-5420; E-mail: rlo@mednet.ucla.edu

can be identified as intrachromosomal complex genomic rearrangements (CGR) and extrachromosomal DNAs (ecDNA, aka double minutes), which may be temporally related structures that confer a range of genomic–signaling plasticity (13). Earlier studies have established the prognostic importance of ecDNAs in clinical tumor tissues and the potential relevance of ecDNAs to therapeutic resistance in cancer cell lines (14, 15). The non-Mendelian inheritance of ecDNAs, their accessible chromatin, as well as enhancer hijacking and transcriptional hub congregation by ecDNAs are all mechanisms that facilitate rapid adaptations to extreme stress such as oncogene-targeted therapy (16–19). Finally, iterative cycles of CGR and ecDNA biogenesis drive the amplification of a model resistance gene (*DHFR*) to the chemotherapy methotrexate (20).

To test the hypothesis that chromothripsis, CGRs, and ecDNAs play key roles in the evolution of MAPKi resistance in clinical melanoma, we analyzed by whole-genome sequencing (WGS) three tumor cohorts (along with patient-matched normal tissues): (i) patient-matched pre-MAPKi and acquired MAPKi-resistant tumors from patients with *BRAF*[V600MUT] melanoma, (ii) acquired MAPKi-resistant melanoma metastatic to multiple organ sites (including the brain) from rapid autopsies of deceased patients with *BRAF*[V600MUT] melanoma, and (iii) acquired MEKi-resistant melanoma and untreated melanoma from *BRAF*[V600MUT] and, importantly, *NRAS*[MUT] melanoma PDXs. We evaluated (i) resistance-specific recurrence of amplicons harboring known and putative resistance-driver genes in CGRs and ecDNAs, (ii) overlaps in the genomic coordinates between CGR–ecDNAs and chromothripsis, and (iii) inferred double-stranded DNA break (DSB) repair pathway(s) based on analysis of breakpoint–junctional sequences of CGR and ecDNA amplicons. Using human melanoma cell lines and PDXs, we tested the efficacy and dissected the mechanisms of blocking genomic instability via targeting of NHEJ-mediated DSB repair to prevent the evolution of acquired MAPKi resistance in both *BRAF*[V600MUT] and *NRAS*[MUT] melanoma.

RESULTS

Advanced Cutaneous Melanoma Cohorts and WGS Data Characteristics

To date, mutational profiles of acquired MAPKi resistance (in patients with *BRAF*[V600MUT] melanoma and treated with BRAFi or BRAFi + MEKi therapy) have been limited to whole-exome analysis (5, 7–9, 21). Thus, we assembled three cohorts of tissues (Supplementary Table S1) for WGS-based analysis of SVs (Supplementary Table S2). The first cohort consisted of patient-matched normal tissues as well as *BRAF*[V600MUT] melanoma tumors before MAPKi therapy and, after initial responses, at disease progression ($n = 10$ normal tissues; $n = 10$ pretreatment tumors; $n = 17$ acquired-resistant tumors; $n = 10$ patients). The second cohort consisted of rapid autopsy melanoma (RAM) tissues ($n = 3$ normal tissues; $n = 1$ sensitive *BRAF*[V600MUT] tumor; $n = 12$ acquired resistant tumors; $n = 3$ deceased subjects who were treated with MAPKi; $n = 6$ metastatic organ sites). The third cohort consisted of *BRAF*[V600MUT] or *NRAS*[MUT] PDX tumors. We subjected PDXs ($n = 6$ models; 1 *BRAF*[MUT] and 5 *NRAS*[MUT] models) to MAPKi therapy in NOD-scid *IL2R* gamma null

(NSG) mice at doses sufficient to elicit tumor regression and then generated acquired MAPKi-resistant tumors ($n = 6$ vehicle-treated tumors; $n = 12$ acquired-resistant tumors; $n = 6$ normal tissues; Supplementary Fig. S1A; refs. 11, 22). Sequencing depths across MAPKi-sensitive/naive tumors (mean, 38×; median, 32×; range, 18–94×), acquired-resistant tumors (mean, 33×; median, 27×; range, 11–85×), and patient-matched normal tissues (mean, 38×; median, 33×; range, 12–98×) were comparable. The median numbers of genetic alterations [somatic single-nucleotide variants (SNV), indels (ID), and copy-number variations (CNV)] for sensitive and resistant tumors were, respectively: (i) 81 SNVs/megabase (Mb), 5 IDs/Mb, and 261 CNVs/genome and (ii) 97 SNVs/Mb, 7 IDs/Mb, and 253 CNVs/genome.

Recurrence, Quantity, Chromosomal Origin, and Complexity of ecDNAs and CGRs in Acquired-Resistant versus MAPKi-Naive Melanoma

Using WGS data, we reconstructed ecDNA- and CGR-derived, high copy-number (CN) amplicons in 58 *BRAF*[V600MUT] and *NRAS*[MUT] MAPKi-sensitive/naive and acquired-resistant tumors ($n = 17$ sensitive tumors; $n = 41$ acquired-resistant tumors; $n = 19$ patients). We detected ecDNAs and CGRs at a highly recurrent rate: ~70% of sensitive and ~77% of acquired-resistant genomes (Supplementary Table S3). With all three cohorts combined, we observed a greater number of ecDNAs and CGRs in acquired-resistant (versus sensitive) genomes (acquired-resistant: $n = 941$ total, $n = 31$ average per tumor; sensitive: $n = 241$ total, $n = 16$ average per tumor; unpaired Student t test, $P = 0.09$; Fig. 1). In a patient-matched analysis of the clinical cohort, 12 of 15 pairwise comparisons showed a higher number of ecDNA and CGR amplicons in acquired-resistant genomes (Wilcoxon test, $P = 0.033$; Supplementary Fig. S1B). Overall, chr7p (26 of 53 genomes) and chr7q (23 of 53 genomes) emerged as hotspots (fragile sites) for CGR and ecDNA amplicon formation (Fig. 1). In addition, we observed recurrent resistance-associated CGRs in chr9p (8 of 41 resistant tumors across all three clinical–autopsy–PDX cohorts) and lower-frequency resistance-associated CGRs (in 2q, 4q, 6p, 8q, 9q, 10q, 18p, 22p, Xp) and ecDNAs (in 6q, 10p). In the total cohort, regardless of whether the tumor was sensitive or resistant to MAPKi, the number of rearranged segments was higher within ecDNAs (versus CGRs; $P = 3.5e-08$, unpaired Student t test; Supplementary Fig. S1C), suggesting ecDNAs as highly dynamic foci of genomic instability. Furthermore, the mean number of rearranged segments (ecDNAs + CGRs) was highest in the RAM (~10 segments per tumor) followed by the clinical (~5 segments per tumor) and PDX (~4 segments per tumor) cohorts (Supplementary Fig. S1D; Kruskal–Wallis rank test, $P = 0.01$). This may reflect the highly advanced evolutionary state of terminal metastatic melanoma in the RAM cohort. Polyploidy has been associated with the onset of chromothripsis (12). Accordingly, we observed higher numbers of CGRs and ecDNAs in genomes with higher ploidy (Supplementary Fig. S1E).

CGR and ecDNA Amplicons Drive MAPKi Resistance

Analysis of amplicons due to intrachromosomal CGRs and ecDNAs uncovered a significant (unpaired Student
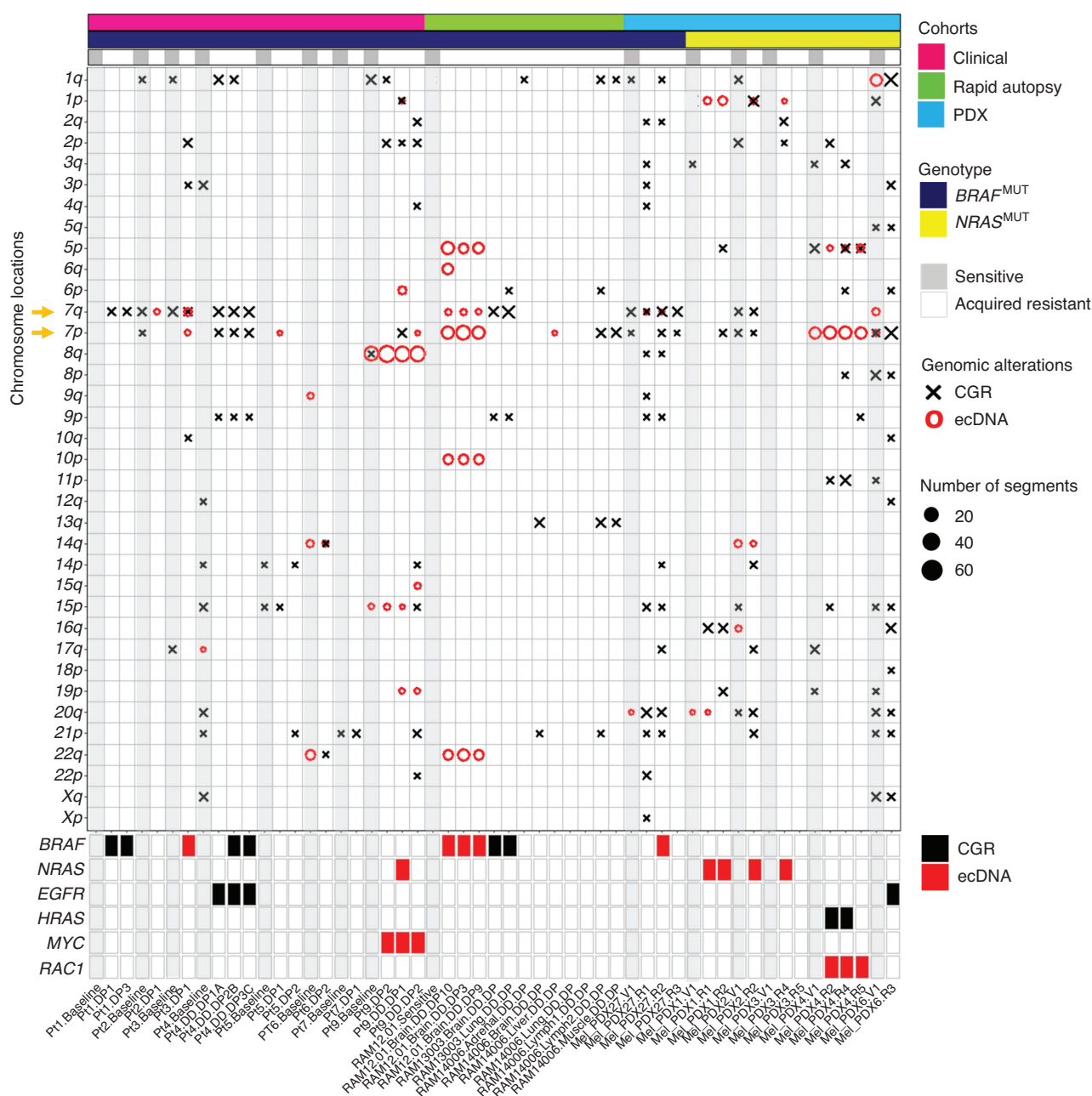
Figure 1. Landscape of ecDNAs and CGRs in patient-matched MAPKi-sensitive and acquired resistant melanoma. Chromosomal distribution of ecDNA and CGR amplicons in three cohorts: $BRAF^{V600MUT}$ clinical cohort (baseline tumors, $n = 8$; resistant tumors, $n = 11$; patients, $n = 8$), RAM tissues (sensitive tumor, $n = 1$; resistant tumors, $n = 12$; deceased patients, $n = 3$), and PDXs (vehicle-treated or sensitive, $n = 6$; resistant tumors, $n = 12$; patients of origin, $n = 6$). Os and Xs, ecDNAs and CGRs, respectively; sizes, numbers of CN variant segments (minimal CN of 4.5; reference sizes shown). Pretreatment and post–acquired resistance tumors from Pt10 and Pt11 are not shown given no detection of ecDNAs and CGRs.

t test, $P = 0.0002$) association between acquired-resistant tumors and CGRs/ecDNAs harboring bona fide MAPKi resistance–driver genes. $BRAF$ (CN range, 4.5–27), $NRAS$ (CN, 5–13), $HRAS$ (CN, 13–16), MYC (CN, 12–15), and $EGFR$ (CN, 4.6–5; Figs. 1 and 2A–D) when amplified are known to drive acquired MAPKi resistance and MAPK pathway reactivation (5, 7–9, 11). $RAC1$ (CN, 6–7) in an ecDNA amplicon was specifically observed in acquired resistance in $NRAS^{MUT}$ melanoma PDXs, which suggests regulation of MLK3–CRAF

by RAC1 (23). Moreover, we validated a recurrent ecDNA by direct isolation and high-depth sequencing [$NRAS$ amplification, CN 13, Pt9-double drug-disease progression (DD-DP)1; Fig. 2A] using a new approach referred to as CRISPR-CATCH (24). This alternative technique confirmed the circularized junctions of an 890-kb driver ecDNA within this acquired-resistant clinical tumor sample. In addition, we used DNA-FISH to validate the resistance-specific presence and the CNs of $BRAF$ and $NRAS$ amplicons (Fig. 2E). In total, among the 17
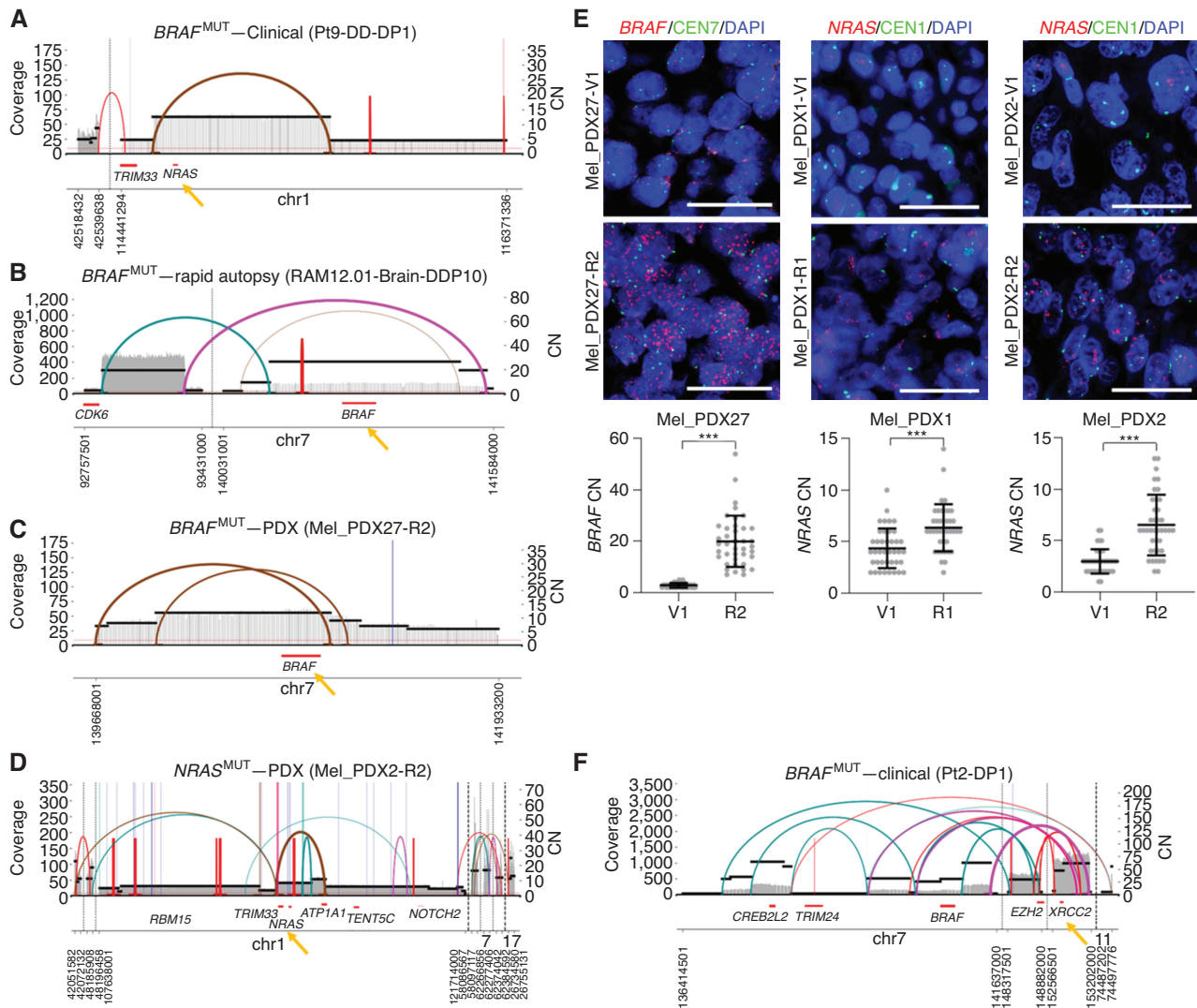
Figure 2. Genes amplified by ecDNAs and CGRs in acquired MAPKi resistance and enriched pathways. **A–D,** SV view of reconstructed amplicons in representative acquired MAPKi-resistant melanoma tumors in the clinical (**A**), RAM (**B**), $BRAF^{V600MUT}$ PDX (**C**), and $NRAS^{MUT}$ PDX (**D**) cohorts. Horizontal black and red lines indicate, respectively, genomic segments with similar CNs and genes. Short vertical lines and arcs indicate discordant read pairs linking two amplicons via an SV junction. Long vertical lines indicate break ends that map from amplicon into low-complexity regions that cannot be traced further. Each line/arc representing discordant reads is colored based on differences from expected distance or orientation. Yellow arrows point out resistance-driver genes within ecDNAs. DD-DP, double drug (BRAFi + MEKi)-disease progression. **E,** Representative images of DNA-FISH showing indicated patient-matched tumors ($n = 3$ pairs) and CNs of $BRAF$ or $NRAS$ in either vehicle-treated/MAPKi-sensitive (top) or acquired MAPKi-resistant (middle) melanoma. CEN, centromere; DAPI, nuclear stain. Scale bars, 25 µm. Quantification of DNA-FISH (bottom) from 40 nuclei per tumor; results shown as mean ± SD. P values (unpaired two-tailed Student t test): ***, $P < 0.001$. **F,** SV view of reconstructed amplicons in clinically acquired resistance showing $XRCC2$ as a putative resistance-driving gene. (*continued on following page*)

of 19 patients included in this study whose tumors harbored ecDNAs/CGRs, MAPK-reactivation genes were amplified via ecDNAs/CGRs specifically in acquired-resistant tumors (but not in any MAPKi-sensitive/naive tumor) at a high frequency (60% or 23 of 38 resistant tumors; Supplementary Table S3). Expectedly, MAPKi resistance–driver gene amplification via ecDNAs/CGRs often co-occurred with other resistance-specific CN alterations and somatic mutations reported earlier (Supplementary Table S4; refs. 7–9). Using tumor-matched RNA-sequencing (RNA-seq) data available from a subset of tumors, CN alterations (resistant versus sensitive)

of MAPK-reactivation genes were highly positively correlated with mRNA level changes (Spearman correlation $r_s = 0.64$, $P = 0.001$; Supplementary Table S5 and Supplementary Fig. S1F). In a minority of patients (Pt5, ecDNA⁺CGR⁺; Pt11, ecDNA⁻CGR⁻; Supplementary Table S6), we observed lower-level but linear amplifications of $BRAF$ (CN, 3–4) specifically in acquired-resistant tumors. The $BRAF^{V600MUT}$ melanoma tumors from both patients were treated with only BRAFi (not BRAFi + MEKi), suggesting that low-level linear amplifications suffice in driving acquired resistance to BRAFi monotherapy.
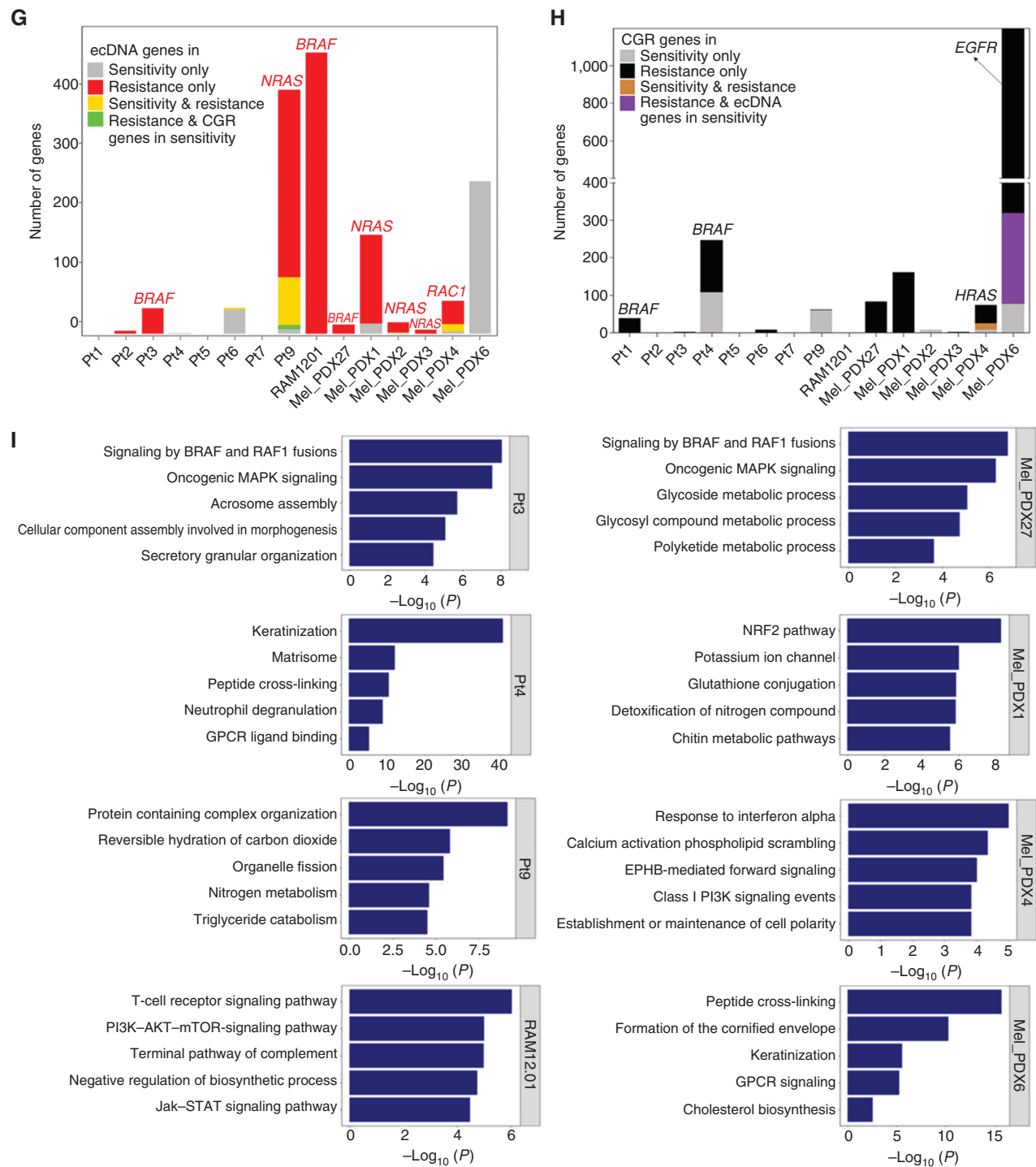
Figure 2. *(Continued)* **G,** Number of ecDNA-amplified genes (i) shared between pre/sensitive and post/acquired resistant tumors, (ii) specifically in pre/sensitive tumors, (iii) specifically in post/acquired resistant tumors, and (iv) in post/acquired resistant tumors shared with CGR-amplified genes in pre/sensitive tumors. Cohorts: clinical (n = 8 patients), RAM (n = 1 patient), and PDX models (n = 6 patients). Patients without sensitivity (n = 2) and without ecDNAs and CGRs detected (n = 2) were excluded. **H,** As in **G,** except showing the number of CGR-amplified genes in the same (i) to (iii). (iv) Number of CGR-amplified genes in post/acquired resistant tumors shared with ecDNA-amplified genes in pre/sensitive tumors. **I,** Pathway enrichment analysis of genes amplified by ecDNAs and/or CGRs exclusively in acquired resistant tumors (n = 8). Only tumors with sufficient genes for enrichment analysis were analyzed. GPCR, G protein-coupled receptor.

Nonhomologous end-joining (NHEJ) and homologous recombination repair (HRR) of DSBs are thought to be critical for CGR and ecDNA generation after chromothripsis (20). Intriguingly, we observed that *XRCC2* (*RAD51-like*; CN, 49), a key HRR gene, and *XRCC6* (*KU70*; CN, 14–15), a key NHEJ gene, were amplified specifically in acquired MAPKi-resistant melanomas as ecDNAs (Fig. 2F; Supplementary Table S3). Moreover, acquired MAPKi resistance was associated with ecDNA or CGR amplicons spanning other DSB repair genes in NHEJ (*TRIM33* CN, 7–11; *PAXIP1* CN, 3) and HRR (*SSBP1* CN, 5; *BRCA2* CN, 6; *RFC3* CN, 6; *TRIM33* CN, 7–11; *SYCP1* CN, 7–9, *TRIM24* CN, 5–11) pathways (Supplementary Table S3). Thus, acquired MAPKi resistance is specifically associated with CGR and ecDNA amplicons in MAPK-reactivation and DSB repair genes, which suggests functional interplay as codrivers of resistance.

Other resistance-specific genes amplified by ecDNAs and/or CGRs may also contribute functionally to the resistant phenotype. Therefore, we identified the genes and their CNs in ecDNA (Fig. 2G) or CGR (Fig. 2H) amplicons specifically associated with sensitivity, resistance, or both. Importantly, genes amplified by either ecDNAs or CGRs specifically in resistance highly outnumbered those specific to sensitive tumors, which indicates that gene amplification by ecDNAs and CGRs contributes to disease progression on MAPKi therapy. Moreover, genes amplified by either ecDNAs or CGRs in both sensitive plus resistant tumors constituted a very small fraction, which is also consistent with the notion that gene amplification by ecDNAs and CGRs contributes to disease progression. We rarely detected overlapping genes in patient-matched sensitivity-associated CGRs and resistance-associated ecDNAs (and vice versa; Fig. 2G and H). To explore the functional contributions of ecDNA- and CGR-amplified genes to the acquired MAPKi-resistant phenotype, we performed pathway enrichment analysis using genes amplified by ecDNAs/CGRs specifically detected in resistance from eight evaluable cases (see Methods; Fig. 2I). This analysis nominated alterations in MAPK (in Pt3, PDX27), PI3K–AKT (RAM12.01, PDX4), immune (Pt4, RAM12.01, PDX4), G protein-coupled receptor (GPCR; Pt4, PDX6), cellular differentiation/morphogenesis (Pt3, Pt4, Pt9, PDX4, PDX6), and metabolism (Pt9, RAM12.01, PDX27, PDX1, PDX6) pathways as resistance phenotypes driven by ecDNAs/CGRs (Supplementary Table S7).

Recent studies have suggested that enhancers within ecDNAs influence oncogene expression by either coamplification with target oncogenes within the ecDNAs (i.e., *cis* interaction) or regulation of intrachromosomal genes (i.e., *trans* interaction; refs. 16, 25, 26). Thus, we annotated CGR and ecDNA amplicons in both sensitive and acquired resistant genomes with enhancers listed in GeneHancer (27). Notably, MAPKi-resistance genes (e.g., *BRAF*, *NRAS*, *HRAS*, and *EGFR*) and known oncogenes (e.g., *EZH2*, *CREB3L2*, *CARD11*, and *EP300*) were coamplified with their corresponding enhancers within CGRs and ecDNAs of MAPKi-resistant genomes (Supplementary Fig. S1G and Supplementary Table S8). We also observed enhancers and associated DSB repair genes, such as *XRCC2*, *XRCC6*, and *RAD21*, within close proximity (−0.5 kb to +1.1 kb; Supplementary Fig. S1G and Supplementary Table S8). Furthermore, 10 of 11 and 4 of 5 acquired-resistant genomes with CGR/ecDNA-associated *BRAF* and

NRAS amplifications, respectively, harbored coamplification of superenhancers (Supplementary Table S8), which suggests that genomic plasticity may facilitate epigenomic plasticity and alter gene expression on a large scale in MAPKi-resistant tumors. In further support of ecDNAs playing a role in epigenomic plasticity, we observed that H3K27 acetylated genomic regions (extracted from ENCODE data) were rearranged to the proximity of and coamplified with ecDNA genes (e.g., *c-MYC* and *BRAF*, respectively) in acquired resistance (Supplementary Fig. S1H). Enhancer docking sites within ecDNA amplicons may also influence the differentiation state(s) of MAPKi-resistant tumors by acting in *trans* on intrachromosomal genes such as *HOXA9*, *HOXA11*, *HOXA13*, and *LIFR* (RAM12.01-Brain-DD-DP10, RAM12.01-Brain-DD-DP3, and RAM12.01-Brain-DD-DP9) and acting as mobile regulatory elements for genes such as *SMO* (Pt3-DP1; Supplementary Table S8) and *ATP1A1* (Mel_PDX2-R2; Supplementary Fig. S1G). Thus, CGR and ecDNA amplicons coamplify MAPKi resistance–specific and –driver genes with their enhancers and may harbor additional enhancer or superenhancer activities in *cis* or *trans* that concomitantly reprogram the transcriptome of acquired resistance.

Pervasive Chromothriptic Genomic Spans in Melanoma Overlap with Genomic Coordinates of ecDNAs and CGRs

Chromothripsis, defined as a mutational phenomenon leading to extensive genomic rearrangements and extensive CN oscillations, drives cancer initiation and progression (12). Prior studies have colocalized chromothriptic regions with ecDNAs (20, 28–30), and a recent study suggested chromothripsis as a pathway for ecDNA formation in general (30) and specifically in ecDNA-driven methotrexate resistance (20). To evaluate the specific contributions of chromothripsis before and after evolution of MAPKi resistance, we analyzed WGS data (Supplementary Table S2) from 58 patient-matched, *BRAF*^V600MUT or *NRAS*^MUT MAPKi-sensitive/naive and acquired-resistant tumors [along with 19 patient-matched normal genomic DNAs (gDNA)]. We observed a high prevalence of chromothripsis (high-confidence calls based on recently published criteria; ref. 12) in MAPKi-sensitive (16 of 17; mean total span per genome, 464 Mb) and acquired-resistant (40 of 41; mean total span per genome, 476 Mb) melanomas. The chromosome distributions of chromothripsis overlapped but were distinct between sensitive and acquired-resistant genomes (Supplementary Fig. S2A and S2B). Chromothriptic genomic spans in MAPKi-sensitive/naive and acquired MAPKi-resistant melanomas overlap 76% and 36%, respectively, with those reported earlier for a subset of The Cancer Genome Atlas skin cutaneous melanoma (12), indicating again that MAPKi selects for chromothripsis in distinct genomic regions. Interestingly, the single MAPKi-sensitive melanoma without chromothripsis (Mel_PDX27-V1) still gave rise to two (of three) acquired-resistant tumors with chromothripsis. The recurrence and span sizes of chromothriptic events in our melanoma cohorts are higher than those reported for cutaneous melanoma in the Pan-Cancer Analysis of Whole Genomes study (mean total span per genome, 120 Mb; ref. 12). These differences may be due to advancing disease and therapy resistance.

If chromothripsis were a precursor step for ecDNA and CGR generation during melanoma disease progression, we expected a nonrandom overlap of affected genomic spans. Consistent with expectation, we observed that the genomic spans of ecDNAs and CGRs overlapped significantly or nonrandomly with chromothriptic regions in ~29% (5 of 17) of MAPKi-sensitive/naive genomes and in ~54% (22 of 41) of acquired MAPKi-resistant genomes (Fig. 3A). For every genome, we computed the sizes of ecDNAs + CGRs ($a - x$), chromothriptic regions ($b - x$), their overlap (x), and genomic regions devoid of these genomic alterations ($g - a - b$). These four quantities were represented in 2×2 contingency tables to carry out the Fisher exact test. Using hypergeometric distribution, we then estimated the probability of observing random overlaps between ecDNA + CGR spans and chromothriptic spans. In each tumor genome with overlaps between ecDNA + CGR and chromothriptic regions, we observed a significant nonrandom convergence (Fisher exact test, $P < 0.00001$), suggesting chromothripsis as an origin of ecDNAs and CGRs (Fig. 3A).

Tumor Mutational Burdens and Single-Base Substitution Signatures of Chromothripsis, ecDNAs, and CGRs

Chromothripsis generation is hypothesized to involve micronuclei, which expose entrapped chromosomes to mutagens and predispose them to replication, transcription, as well as DNA repair defects (31). Therefore, we identified and characterized the somatic SNVs within the chromothriptic regions across the melanoma genomes in our three cohorts. The numbers of chromothripsis-associated SNVs ranged from 31 to 2,526 per Mb (mean 154 mutations/Mb, median 96 mutations/Mb; Supplementary Table S2). We next tested the hypothesis that chromothripsis may disproportionally contribute to the tumor mutational burdens (TMB), especially in acquired-resistant genomes, by calculating the numbers of SNVs within chromothriptic regions relative to the numbers of SNVs within nonchromothriptic regions. Acquired-resistant tumors harbored an average of 195 SNVs/Mb in chromothriptic regions versus an average of 93 SNVs/Mb in nonchromothriptic regions. Because the ratio of the chromothriptic region (~476 Mb) to nonchromothriptic region (~2,619 Mb) is 0.18 and given the TMB of 170 SNVs/Mb in acquired resistance, we expected only 31 SNVs/Mb (0.18×170) in chromothriptic regions of acquired-resistant tumors if SNVs were evenly distributed across the genome. Moreover, MAPKi-sensitive or pretreatment tumors harbored an average of 121 SNVs/Mb in chromothriptic regions versus an average of 84 SNVs/Mb in nonchromothriptic regions. Again, an observed average of 121 SNVs/Mb in chromothriptic regions was higher than the expected 20 SNVs/Mb in the chromothripsis regions, which was calculated based on a 0.17 ratio of the chromothriptic region (~464 Mb) to nonchromothriptic region (~2631 Mb) and the observed average TMB of 115 SNVs/Mb in MAPKi-sensitive tumors. Hence, in both acquired-resistant and MAPKi-sensitive melanoma genomes, chromothriptic regions were enriched for SNVs compared with nonchromothriptic regions (Fisher exact test, $P < 0.00001$). Furthermore, the ratio of SNVs in chromothriptic to nonchromothriptic genomes was higher in acquired-resistant versus MAPKi-naive/sensitive tumors (Wilcoxon rank sum test, $P = 0.005$; Supplementary Fig. S2C), suggesting that MAPKi-selected chromothriptic regions in some individuals feature a relatively stronger mutator phenotype.

We have reported that MAPKi selection of clinical melanomas alters the mutational spectra (9). To characterize how a MAPKi-associated mutator phenotype affects chromothriptic genomic spans selected by MAPKi, we culled chromothripsis-associated somatic mutations unique to MAPKi-sensitive/naive (mean, 64 SNVs/Mb) versus MAPKi-resistant genomes (mean, 58 SNVs/Mb) and analyzed signatures of single-base substitutions (SBS; Fig. 3B), double-base substitutions (DBS), and IDs (Supplementary Fig. S2D; 32, 33). In both MAPKi-sensitive/naive and acquired-resistant tumors, we frequently detected signatures of tobacco smoking (SBS4) and ultraviolet radiation (SBS7a and SBS38). Among chromothripsis-associated somatic mutations unique to either MAPKi-sensitive/naive or acquired-resistant tumors, we also detected a signature of defective HRR (SBS3), and this trended higher in resistant (12 of 31) versus sensitive (3 of 16) tumors, although this difference was not significant. Unique but infrequent to acquired MAPKi resistance was the detection of mutational signatures of polymerase eta somatic hypermutation (SBS9) and defective POLD1 proofreading activity (SBS10d, SBS20). Unique and recurrent in acquired MAPKi resistance was the detection of mutational signatures of (i) defective DNA mismatch repair (MMR; SBS6, SBS20, SBS26, and SBS44; 14 of 31 resistant tumors; 10 of 16 patients) and (ii) defective base excision repair (BER) as well as damage due to reactive oxygen species (ROS) or mutations in *NTHL1* and *MUTYH* (SBS18, SBS30, and SBS36). As exceptions, SBS26 and SBS36 signatures were also detected at a low percentage in two sensitive tumors (one of which had been exposed to MAPKi). BER/ROS signatures were observed more frequently in the *BRAF*^{V600MUT} (10 of 22 resistant tumors, 6 of 11 patients) than in the *NRAS*^{MUT} (1 of 9 resistant tumors, 1 of 5 patients) subset. This differential frequency may be due to the longer MAPKi exposure in the clinical (versus PDX or experimental) setting. Consistently, the BER mutational signature (SBS18) was detected in Mel_PDX3-R5, which was among the acquired-resistant PDX tumors with longer durations of MAPKi treatment (Supplementary Fig. S1A). Overall, resistance-specific (versus sensitivity-specific) chromothriptic somatic SBSs enriched for signatures of defects in BER (Wilcoxon rank sum test, $P = 0.04$) and MMR (Wilcoxon rank sum test, $P = 0.005$). Moreover, resistance-specific (versus sensitivity-specific) nonchromothriptic SBSs also enriched for signatures of defects in BER (Wilcoxon rank sum test, $P = 0.05$), MMR (Wilcoxon rank sum test, $P = 0.008$), as well as HRR (Wilcoxon rank sum test, $P = 0.04$; Supplementary Table S9). We did not identify any resistance-specific or -enriched DBS and ID signature (Supplementary Fig. S2D).

We also identified SBS signatures within ecDNA and CGR sequences and determined whether certain SBS signatures are enriched in acquired MAPKi-resistant (versus MAPKi-sensitive/naive) tumors or ecDNA/CGR amplicons (versus noninvolved genomic regions regardless of tumor sensitivity or resistance; Fig. 3C). We extracted somatic SNVs unique to MAPKi-sensitive/naive ($n = 12$) and acquired-resistant ($n = 28$) tumors (in a patient-matched fashion) within
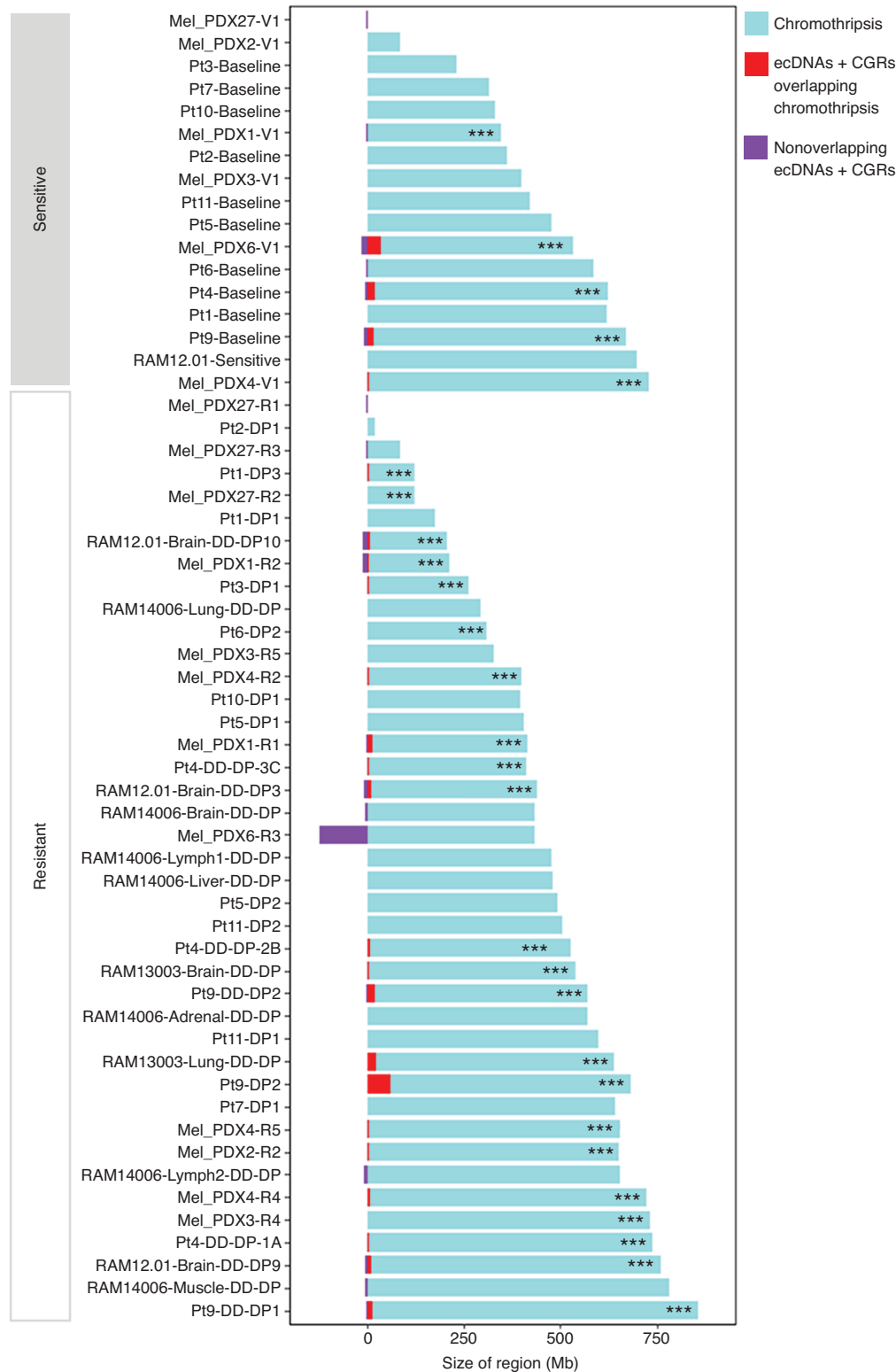
A

Figure 3. Associations of chromothripsis, ecDNAs, and CGRs with mutagenic and double-stranded DNA repair pathways. **A,** Pattern of overlap or nonoverlap between ecDNA + CGR and chromothriptic genomic spans within individual sensitive ($n = 17$; top) and acquired resistant ($n = 41$; bottom) melanoma tumors. Sizes (Mb) of chromothriptic regions are in cyan, ecDNAs + CGRs overlapping with chromothripsis in red, and ecDNAs + CGRs nonoverlapping with chromothripsis in purple. *P* value (Fisher exact test) of nonrandom overlap between chromothriptic and ecDNA + CGR regions: ***, $P < 0.00001$. (*continued on following page*)
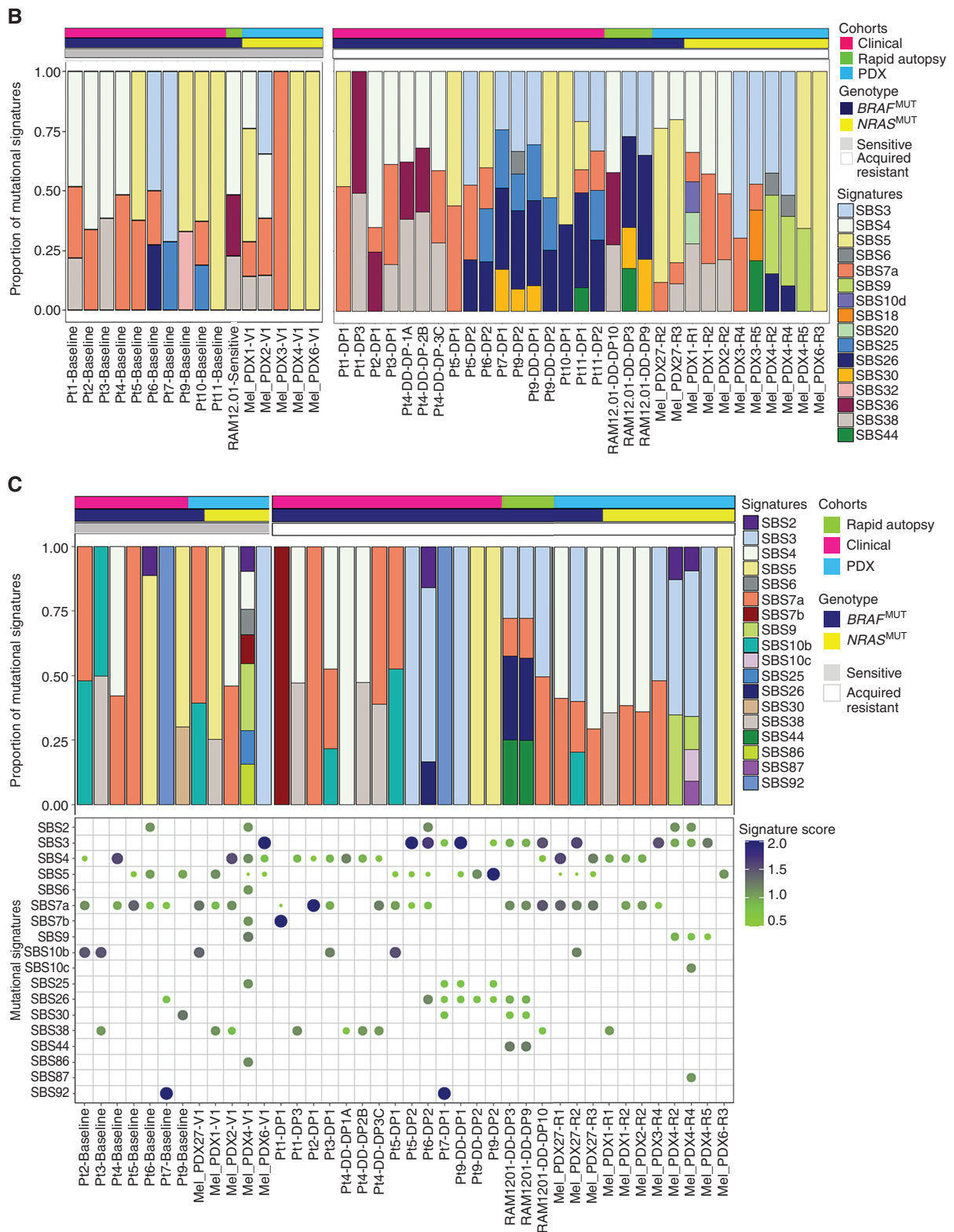
Figure 3. *(Continued)* **B,** SBS signatures of chromothriptic genomes of MAPKi-sensitive/naive (left, *n* = 16) versus MAPKi-resistant (right, *n* = 31) melanoma tumors. Excluded from analysis, acquired resistant tumors without patient-matched sensitive tumors and tumors without chromothripsis. **C,** Top, SBS signatures of ecDNAs + CGRs of MAPKi-sensitive/naive (left, *n* = 12) versus MAPKi-resistant (right, *n* = 28) melanoma tumors. Bottom, SBS signature enrichment scores are shown by both heat scale and dot size. Increasing dot sizes indicate increasing enrichment of indicated signatures within ecDNAs + CGRs compared with regions devoid of these events (score > 1). Enrichment score = 1 is considered the cutoff; only scores >1 and <1 are shown. Excluded from analysis are acquired-resistant tumors without patient-matched sensitive tumors and tumors without ecDNAs and CGRs. *(continued on next page)*
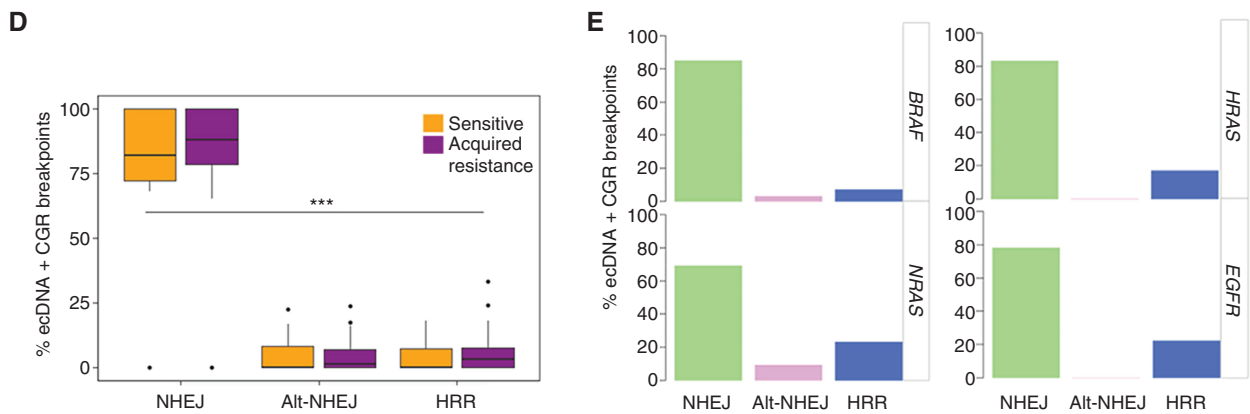
Figure 3. *(Continued)* **D,** Breakpoint–junctional sequence analysis of ecDNAs + CGRs inferring indicated DNA DSB repair processes: NHEJ, alternative NHEJ (alt-NHEJ), and HRR. Amplicons from all three cohorts of tumors combined for analysis (sensitive, $n = 17$; resistant, $n = 41$). Homologous sequences of size 0–1 bp (NHEJ), 2–8 bp (alt-NHEJ), and >8 bp and large insertions (HRR). ***, P value (Kruskal–Wallis test) = 6.35e−16. **E,** As in **D,** except only for resistant tumor–derived ecDNA and CGR amplicons that harbor *BRAF* ($n = 11$), *NRAS* ($n = 5$), *HRAS* ($n = 2$), and *EGFR* ($n = 4$) genes.

ecDNA/CGR amplicons. CGR + ecDNA-associated TMB trended higher in acquired-resistant (mean, 130 SNVs/Mb) compared with MAPKi-sensitive/naive (mean, 80 SNVs/Mb) tumors (Wilcoxon rank sum test, $P = 0.06$). Enrichment of SBS3 (defective HRR) was more recurrent in the ecDNAs/CGRs of resistant tumors (11 of 28) compared with patient-matched sensitive tumors (1 of 12), although this difference did not reach statistical significance (Wilcoxon rank sum test, $P = 0.08$; Fig. 3C). Moreover, we derived mutational signature enrichment scores by calculating the normalized ratios of signature proportions within ecDNAs/CGRs and within regions devoid of these events (scores >1 defined as positive enrichment; see Methods). We found that 25% (7 of 28) of acquired-resistant tumors displayed positive enrichment scores for defective HRR signatures (SBS3) within ecDNAs and CGRs, whereas only 8% (1 of 12) of sensitive tumors displayed positive enrichment (Wilcoxon rank sum test, $P = 0.3$; Fig. 3C). In either sensitive or resistant tumors, we observed positive enrichment scores for SBS signatures reflective of APOBEC cytidine deaminase activity (SBS2; 2 of 12 in sensitivity; 3 of 28 in resistance) and polymerase epsilon exonuclease domain mutations (SBS10b; 3 of 12 in sensitivity; 3 of 28 in resistance). Positive enrichment scores were also noted with lower recurrence for SBS signatures of defective POLD1 proofreading (SBS10c), defective MMR (SBS44), chemotherapy treatment (SBS86, SBS87), and tobacco smoking (SBS82). Overall, 50% (6 of 12) of sensitive/naive and 32% (9 of 28) of acquired-resistant tumors displayed enrichment of unique SBS signatures within ecDNA + CGR sequences compared with uninvolved genomic regions. Lastly, we addressed whether the enrichment of unique SBS signatures differed within ecDNAs versus CGRs in acquired resistance (Supplementary Fig. S2E). We observed positive enrichment scores of SBS2 (APOBEC cytidine deaminase activity) in 26% (5 of 19) of ecDNA+ acquired-resistant tumors compared with 4% (1 of 24) of CGR+ acquired-resistant tumor (Wilcoxon rank sum test, $P = 0.05$; Supplementary Fig. S2F). This finding is consistent with the recent discovery of the co-occurrence of APOBEC3

kataegis in ecDNAs (33). We also observed positive enrichment scores of SBS3 (defective HRR) in 47% (9 of 19) of ecDNA+ acquired-resistant tumors compared with 17% (4 of 24) of CGR+ acquired-resistant tumors (Wilcoxon rank sum test, $P = 0.07$; Supplementary Fig. S2F). In short, ecDNA and CGR amplicons, whether in MAPKi-sensitive/naive or acquired-resistant tumors, harbor SBS patterns suggestive of specific defects or deficiencies in HRR. In acquired MAPKi resistance, APOBEC activity likely contributes to ecDNA mutagenesis and hence shapes the mutanome of ecDNA amplicons. Further analysis might lead to insights into ecDNA biogenesis and suppressive strategies.

NHEJ Underlies the Formation of ecDNAs and CGRs

We analyzed the breakpoint–junctional sequences of CGRs and ecDNAs to infer DSB repair processes underlying resistance-associated amplicons (Fig. 3D). Alternative end-joining refers to mechanisms of DSB repair that may compensate for HRR- and NHEJ-based repairs and comprises single-strand annealing (SSA), microhomology-mediated end-joining (MMEJ), and other end-joining pathways (34). SSA is indicated in the breakpoint junctions by complementary repeat sequences >25 nucleotides and MMEJ by shorter tracks of sequence homology (2–20 nucleotides). Moreover, replicative processes, such as fork stalling and template switching as well as MMEJ, can contribute to the generation of CGRs. Breakpoint junctions derived from replicative processes (e.g., replicative fork collapsing when it encounters a nick) are expected to have microhomologies, insertions, and relatively long templated insertions (35, 36). Indeed, signatures of replication processes and templated insertion, as well as that of NHEJ, were detected pan-cancer (12). Analysis of breakpoint–junctional sequences of all resistance- and sensitivity-associated CGRs and ecDNAs inferred NHEJ as the main mechanism of double-stranded DNA fragment joining or rearrangement (Fig. 3D; Supplementary Fig. S3A). A lower number of breakpoint–junctional sequences displayed short and long homologous sequences as well as insertions (>10 bp), which

suggested DSB repair by alternative NHEJ (alt-NHEJ) and HRR, respectively (Fig. 3D). Analysis of breakpoint–junctional sequences of specifically ecDNAs and CGRs harboring MAPK-reactivation or MAPKi resistance–driver genes also revealed a similar pattern, with NHEJ dominating the landscape of DSB repair mechanisms (Fig. 3E). Of unknown significance or etiology, a higher incidence of double-stranded DNA ligation by HRR was detected in *NRAS*^{MUT} melanoma, either sensitive or acquired-resistant to MAPKi, compared with *BRAF*^{V600MUT} melanoma (Supplementary Fig. S3B). In acquired-resistant genomes, we also detected a higher incidence of double-stranded DNA ligation by NHEJ for CGRs compared with ecDNAs (Supplementary Fig. S3C).

Inhibitors of DNA-PK$_{CS}$ and/or PARP1/2 Prevent Acquired MAPKi Resistance in Melanoma Cell Lines

DNA-dependent protein kinase catalytic subunit (DNA-PK$_{CS}$) and PARP1/2 are involved in multiple DSB repair pathways, particularly NHEJ (DNA-PK$_{CS}$), HRR (DNA-PK$_{CS}$, PARP1/2), and MMEJ (PARP1/2; refs. 37, 38). Thus, we tested the activity of the specific DNA-PK$_{CS}$ inhibitor (DNA-PKi) NU7026 and PARP1/2 inhibitor (PARPi) ABT888 (veliparib), individually and combinatorially, in preventing the clonal emergence of drug-tolerant proliferating persisters (DTPP; refs. 39, 40) from human *BRAF*^{V600MUT} (*n* = 3; M229, M249, M395) or *NRAS*^{Q61MUT} (*n* = 3; M202, M207, M245; Fig. 4) melanoma cell lines chronically treated with BRAFi + MEKi or MEKi, respectively. We hypothesized that DNA-PKi interferes with MAPKi-elicited, *de novo* rearrangement of specific SVs including ecDNAs and CGRs. We further hypothesized that DNA-PKi is more effective at preventing rather than reversing resistance once fully established by chronic MAPKi treatment. Hence, we tested treatments with NU7026 and/or ABT888 in combination with MAPKi in acquired MAPKi-resistant sublines (*n* = 9) that are isogenic to the parental human *BRAF*^{V600MUT} and *NRAS*^{Q61MUT} cell lines (Fig. 4A–O). *BRAF*^{V600MUT} sublines with acquired-resistance to BRAFi + MEKi are annotated as double-drug resistant (DDR), whereas *NRAS*^{MUT} sublines with acquired-resistance to MEKi are annotated simply by their clone (C) numbers. We began by testing the single-agent anticlonogenic growth activity of DNA-PKi and PARPi on parental melanoma (and nonmelanoma, see below) cell lines without MAPKi treatment in order to select noninhibitory concentrations to test in combination with MAPKi (Supplementary Fig. S4A–S4G). In combination with MAPKi, NU7026 synergistically and dose dependently prevented DTPP formation in all parental cell lines tested (Fig. 4A, D, G, I, J, and N), whereas ABT888 displayed activity in 3 of 6 parental cell lines (Fig. 4A, D, and J). In cases in which ABT888 individually was active in preventing DTPP formation, NU7026 plus ABT888 led to even greater suppression of acquired MAPKi resistance (Fig. 4A, D, and J). Consistently in all acquired MAPKi-resistant sublines, NU7026 and ABT888 at the lower range of the concentrations tested displayed no or reduced anticlonogenic activity compared with their activities observed in isogenic parental lines (Fig. 4A–O). More recent generations of DNA-PKi display improved selectivity and potency (37, 41). Hence,

we used next-generation DNA-PKi (VX984 and AZD7648) and PARPi (olaparib) and corroborated their combinatorial efficacy with MAPKi in parental cell lines (Supplementary Fig. S4C–S4E and Supplementary Fig. S5A–S5F). In M245, we further corroborated the pharmacologic findings with genetic studies. Using independent short hairpin RNAs (shRNA) against two critical NHEJ genes (*PRKDC*, which encodes DNA-PK$_{CS}$, and DNA ligase IV, or *LIG4*), we showed that their protein knockdown, while not having a significant effect on growth without MAPKi, strongly suppressed the frequency of DTPP emergence (Fig. 4P and Q).

The acquired-resistant sublines used in the prior experiments have been adapted chronically (i.e., months to years) to MAPKi. Hence, we also tested whether a shorter delay (i.e., weeks) in the cotreatment of parental cell lines with DNA-PKi (and/or PARPi) would hinder the efficacy in preventing DTPP formation. In both cell lines (M229 *BRAF*^{V600MUT} and M245 *NRAS*^{MUT}), we found that a 3- to 3.5-week delay in cotreatment with DNA-PKi and/or PARPi reduced the suppression of resistance (Fig. 4R and S compared with Fig. 4A and J, respectively). In the same parental cell lines, we then compared cotreatment with DNA-PKi (and/or PARPi) during the first versus second half of the overall MAPKi treatment course (Fig. 4T and U). Notably, we observed that cotreatment with DNA-PKi, PARPi, or DNA-PKi + PARPi during the first half of the MAPKi treatment course was remittive and during the second half inferior (compared with continuous cotreatment). Thus, the upfront and initial phase of MAPKi therapy appears to be the key window of opportunity for cotreatment with DNA-PKi (and/or PARPi) to suppress acquired MAPKi resistance, suggesting a preventive mechanism of action.

To support further a causal link between acquired MAPKi resistance and ecDNAs or homogeneously staining regions (HSR) in human melanoma cell lines, we first sought to determine the modes of amplification of bona fide resistance-driver genes. In three parental cell lines (*BRAF*^{V600MUT}, M249 and M395; *NRAS*^{MUT}, M245) and five isogenic acquired MAPKi-resistant sublines, we performed DNA-FISH on cells in metaphase and probed against *BRAF* (amplification of which drives acquired MAPKi resistance in *BRAF*^{V600MUT} melanoma; refs. 5, 7–9), *RAF1*, and *NRAS* (amplification of which drives acquired MAPKi resistance in *NRAS*^{MUT} melanoma; refs. 11, 22), as well as centromeres of chr7, chr3, and chr1, respectively (Fig. 5A–C). We observed in acquired resistance that *BRAF* is amplified either as HSRs (M249 DDR4 and DDR5) or as ecDNAs (M395 DDR), *RAF1* as a mixture of HSRs and ecDNAs (M245 C3), and *NRAS* as HSRs (M245 C5). Expectedly, these driver ecDNAs and HSRs were not detected in the isogenic parental cell lines (Fig. 5A–C). We then tested whether MAPKi withdrawal would select against resistant clones with ecDNAs and/or HSRs that amplify the aforementioned resistance-driver genes and, consequently, restore at least partial MAPKi sensitivity. Importantly, we observed that MAPKi withdrawal from acquired-resistant sublines significantly reduced metaphase cells with driver ecDNAs and HSRs (Fig. 5A–C) and significantly enhanced their MAPKi sensitivity (Fig. 5D–F). Using the M249 parental cell line, which is highly sensitive to resistance suppression by either DNA-PKi or PARPi (Fig. 4D), we tracked the emergence of *BRAF* HSR early on treatment (day 31) with
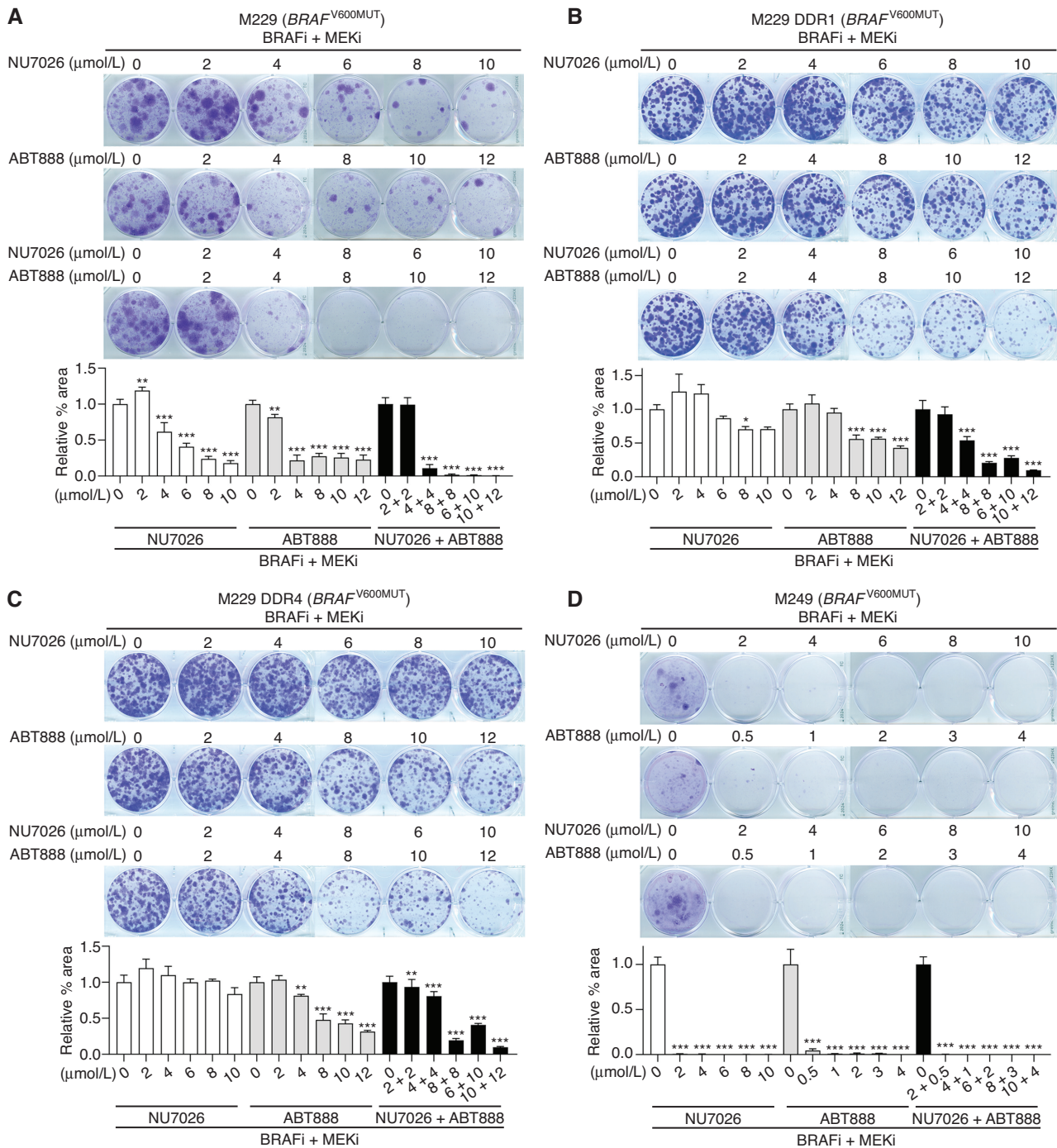
Figure 4. DNA-PKi and/or PARPi cotreatment prevents acquired MAPKi resistance in human melanoma cell lines. **A–O,** Long-term clonogenic growth of isogenic parental and acquired MAPKi-resistant $BRAF^{V600MUT}$ (**A–H**) or $NRAS^{Q61MUT}$ (**I–O**) human melanoma cell lines showing acquired resistant colonies to BRAFi + MEKi (PLX4032 at 0.5 μmol/L, AZD6244 at 0.5 μmol/L in **A** and **G**; PLX4032 at 0.25 μmol/L, AZD6244 at 0.25 μmol/L in **D**; PLX4032 at 1 μmol/L, AZD6244 at 1 μmol/L in **B**, **C**, **E**, **F**, and **H**) or MEKi (trametinib at 0.005 μmol/L in **I** and 0.01 μmol/L in **J** and **N**; trametinib at 0.1 μmol/L in **K**, **L**, **M**, and **O**) and their suppression by indicated cotreatments with DNA-PKi (NU7026) and/or PARPi (ABT888) at indicated concentrations. Top, representative cultures; bottom, quantifications over $n = 4$ fields (mean ± SD). Data representative of 2 to 4 independent repeats. Seeding densities (cells/well in 6-well dishes) and culture durations (days): 5,000; 31 (**A**), 1,000; 17 (**B**), 5,000; 18 (**C**), and 40,000; 40 (**D**). (*continued on following page*)

BRAFi + MEKi or combinations with DNA-PKi, PARPi, or DNA-PKi + PARPi (Fig. 5G). Consistent with *BRAF* HSRs as a driver of acquired MAPKi resistance, we observed their induction by BRAFi + MEKi but suppression by combinatorial treatments with DNA-PKi and/or PARPi. During the earliest window on MAPKi treatment, expansion of ecDNA- and CGR-involved genomic spans may be critical for specific resistance-driving ecDNAs and CGRs to emerge later. We
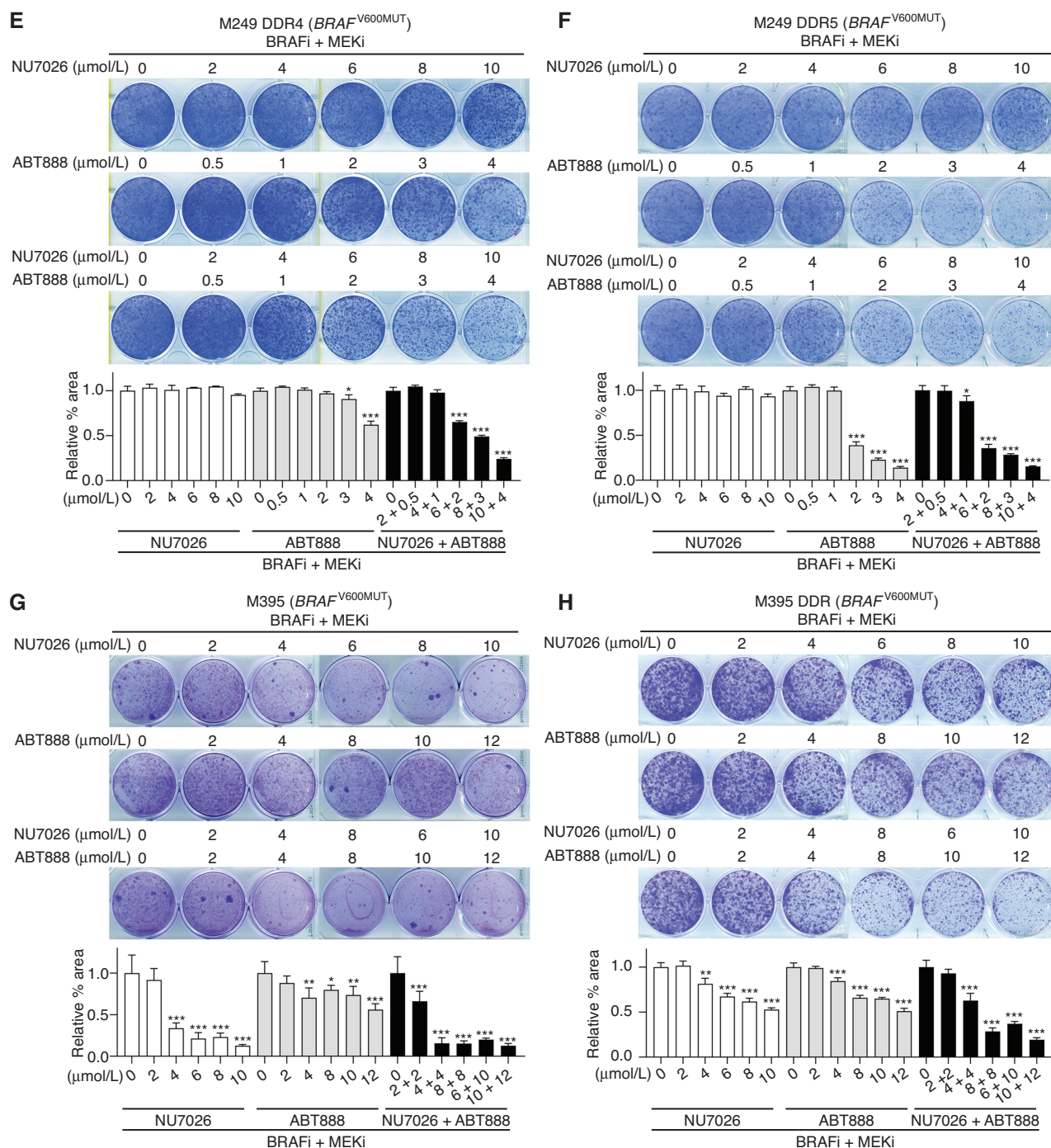
Figure 4. *(Continued)* Seeding densities (cells/well in 6-well dishes) and culture durations (days): 5,000; 14 (**E**), 5,000; 12 (**F**), 20,000; 30 (**G**), and 20,000; 21 (**H**). *(continued on next page)*

reasoned that DNA-PKi, which is generally more effective than PARPi in preventing acquired resistance (Fig. 4), should suppress MAPKi-elicited ecDNA + CGR genomic spans. To test this hypothesis, we performed WGS on two parental cell lines (M229 and M245) treated with vehicle, MAPKi, or MAPKi + DNA-PKi for a short duration (10–11 days); identified ecDNAs and CGRs; and calculated treatment-specific genomic spans of ecDNAs + CGRs (by filtering out

ecDNA and CGR spans detected in vehicle-treated genomes; Supplementary Table S10). Consistent with our hypothesis, DNA-PKi cotreatment with MAPKi blunted the expansion of ecDNA + CGR genomic spans in both cell lines (Fig. 5H). Compared with treatment with MEKi alone, M245 cells treated with MEKi + DNA-PKi gained *de novo* ecDNAs (0.06 Mb in chr3) and lost CGRs (0.4 Mb in chr1 and chr2; Fig. 5H).
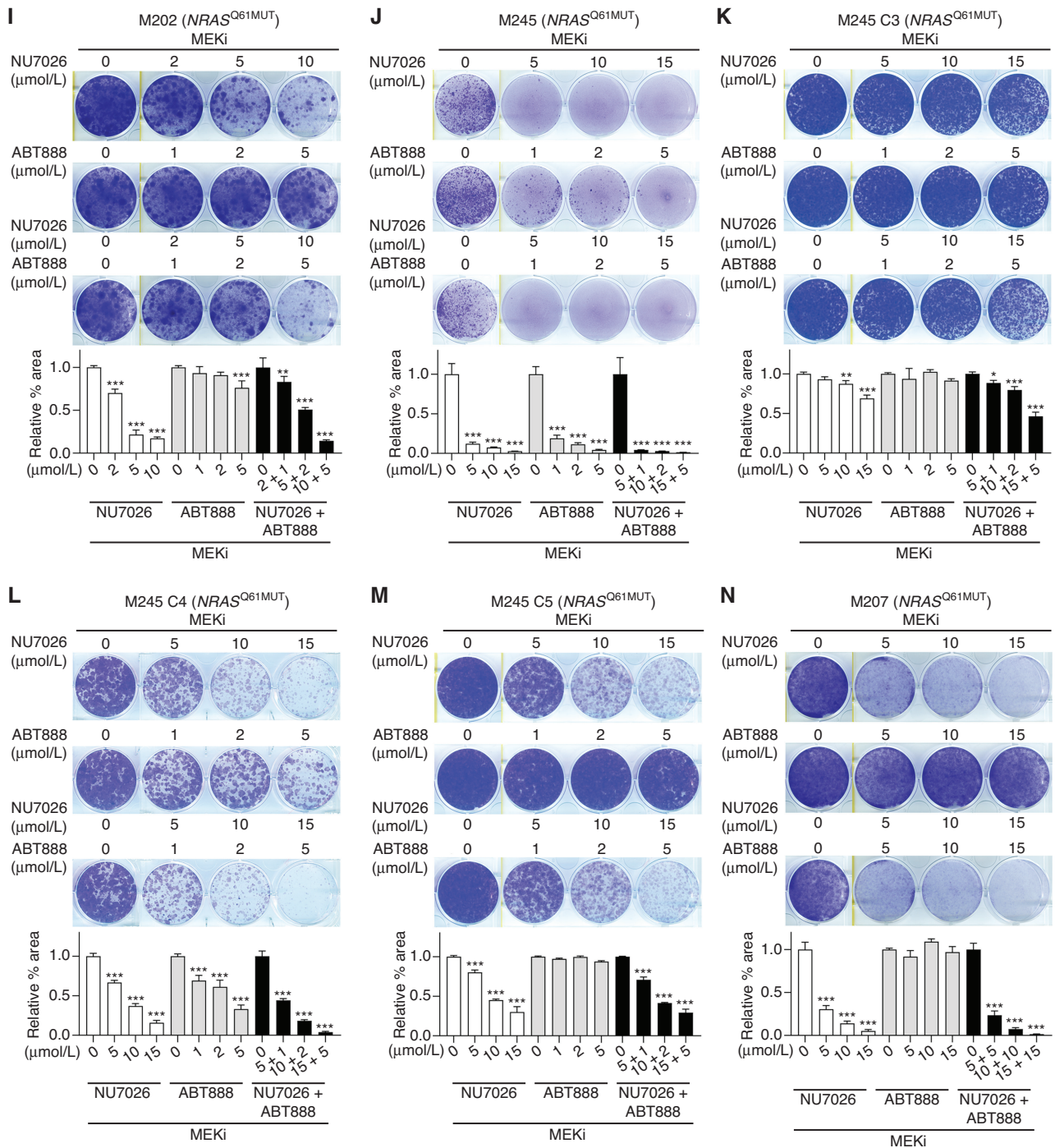
Figure 4. (Continued) Seeding densities (cells/well in 6-well dishes) and culture durations (days): 40,000; 30 (**I**), 50,000; 31 (**J**), 5,000; 17 (**K**), 5,000; 22 (**L**), 5,000; 16 (**M**), and 20,000; 16 (**N**). (continued on following page)

DNA-PKi Suppresses Acquired MAPKi Resistance in $KRAS^{G12C}$ Pancreatic Ductal Adenocarcinoma and Non–Small Cell Lung Carcinoma Cell Lines

As DNA-PKi plus MAPKi may constitute an effective combination for $BRAF^{V600MUT}$ and $NRAS^{MUT}$ melanoma, we explored this combinatorial efficacy (± PARPi) in human pancreatic ductal adenocarcinoma (PDAC) and non–small cell lung carcinoma (NSCLC) cell lines driven by $KRAS^{G12C}$. For

the MAPKi regimen, we used MEKi (trametinib), $KRAS^{G12C}$ inhibitor ($KRAS^{G12C}$i; AMG510 or MRTX849) + MEKi, or type II RAF inhibitor (RAFi; BGB-283) + MEKi. As with melanoma cell lines, we first identified concentrations of DNA-PKi (NU7026) or PARPi (ABT888) that did not affect the clonogenic growth of $KRAS^{G12C}$ PDAC and NSCLC cell lines without MAPKi (Supplementary Fig. S4F and S4G). We then assayed for acquired MAPKi-resistant growth in these cell
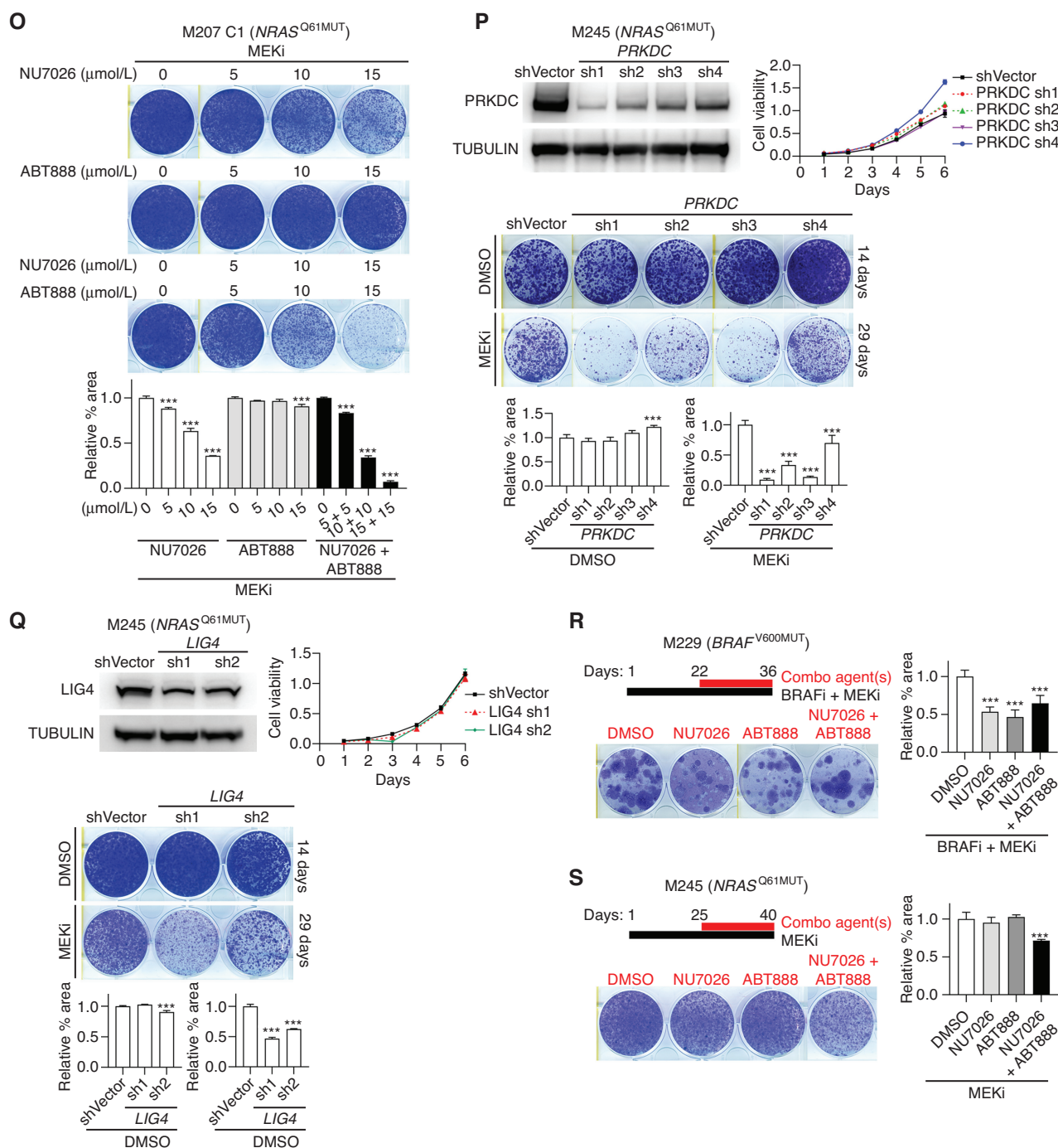
Figure 4. *(Continued)* Seeding density (cells/well in 6-well dishes) and culture duration (days): 5,000; 16 (**O**). Data representative of 2 to 4 independent repeats. **P** and **Q,** Western blot, MTT assay (top right), and clonogenic growth assay (bottom) of M245 cells transduced by lentivirus harboring shVector control or shRNAs of *PRKDC* (**P**) or *LIG4* (**Q**). TUBULIN, loading control. Clonogenic growth with vehicle (14 days, 5,000 cells/well in 6-well dishes) or MEKi (29 days, 50,000 cells/well in 6-well dishes) treatments. MEKi, trametinib at 0.01 μmol/L. Representative results of 2 independent experiments; quantification of $n = 4$ fields (mean ± SD). **R** and **S**, As in **A** and **J**, respectively, except DNA-PKi and/or PARPi cotreatments were performed in M229 (**R**) and M245 (**S**) at a later stage of MAPKi treatment (see time-point schema). Inhibitor concentrations for M229: BRAFi + MEKi (PLX4032 at 0.5 μmol/L, AZD6244 at 0.5 μmol/L), NU7026 (8 μmol/L), ABT888 (4 μmol/L), and NU7026 + ABT888 (4 μmol/L + 4 μmol/L). Inhibitor concentrations for M245: MEKi (trametinib at 0.01 μmol/L), NU7026 (5 μmol/L), ABT888 (1 μmol/L), and NU7026 + ABT888 (5 μmol/L + 1 μmol/L). Left, representative cultures; right, quantifications over $n = 4$ fields (mean ± SD). Data representative of 2 independent repeats. *(continued on next page)*
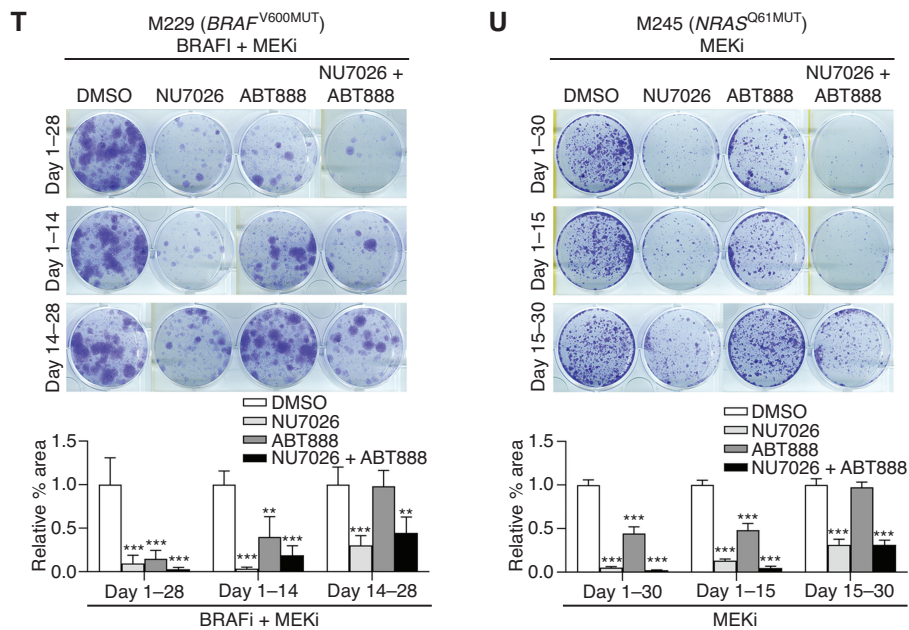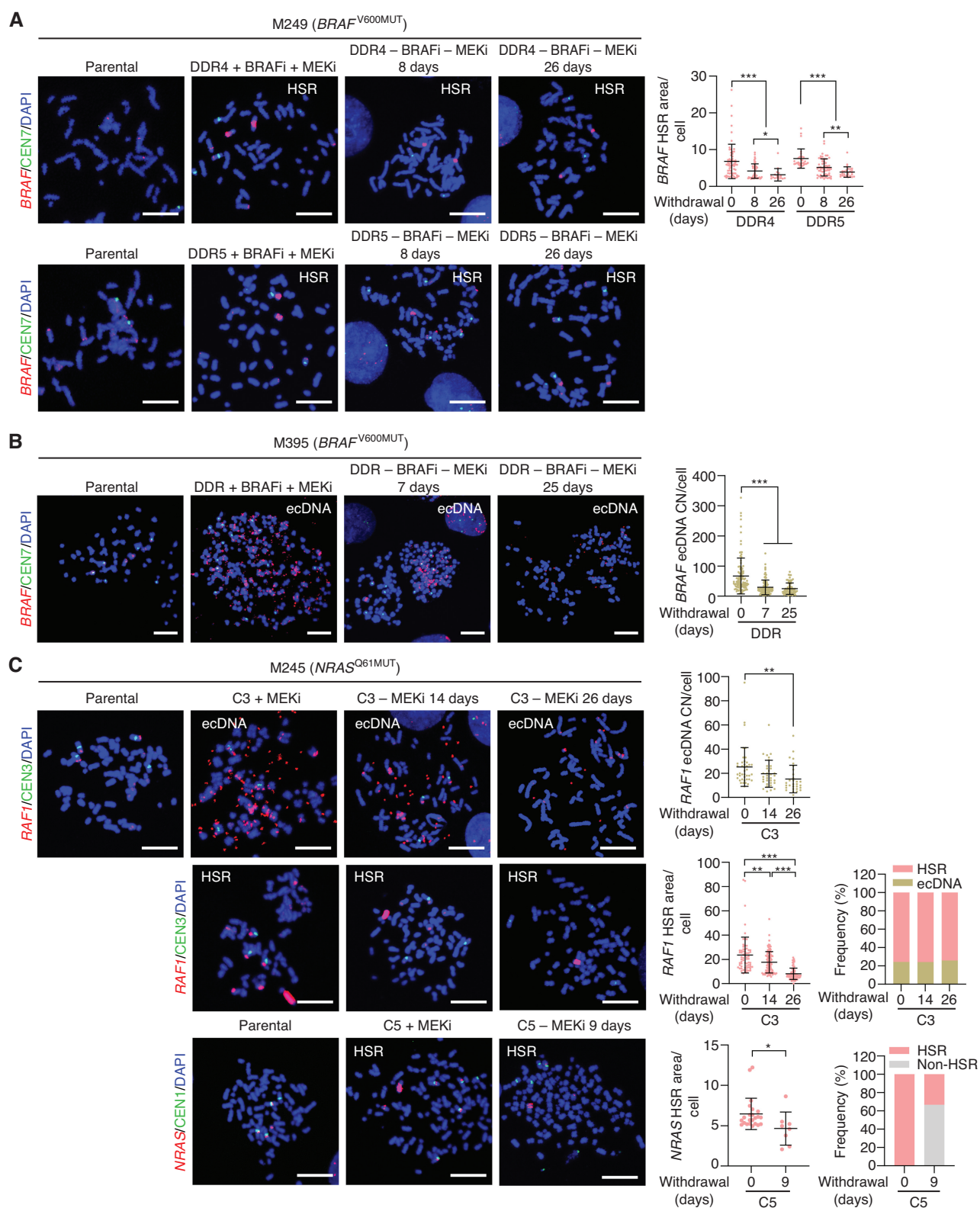
Figure 4. *(Continued)* **T** and **U,** As in **A** and **J,** respectively, except DNA-PKi and/or PARPi cotreatments were performed in M229 (**T**) and M245 (**U**) cells at the same concentrations in **R** and **S** for the entire duration (day 1–28 in **T**; day 1–30 in **U**), the first half (day 1–14 in **T**; day 1–15 in **U**) or the second half (day 14–28 in **T**; day 15–30 in **U**) of the total treatment course. Top, representative cultures; bottom, quantifications over $n = 4$ fields (mean ± SD). Data representative of 2 independent repeats. *P* values (one-way ANOVA followed by the Tukey multiple comparisons test) comparing indicated cultures versus MAPKi-only cultures (**A–O** and **R–U**) or shVector culture (**P** and **Q**): *, $P < 0.05$; **, $P < 0.01$; ***, $P < 0.001$.
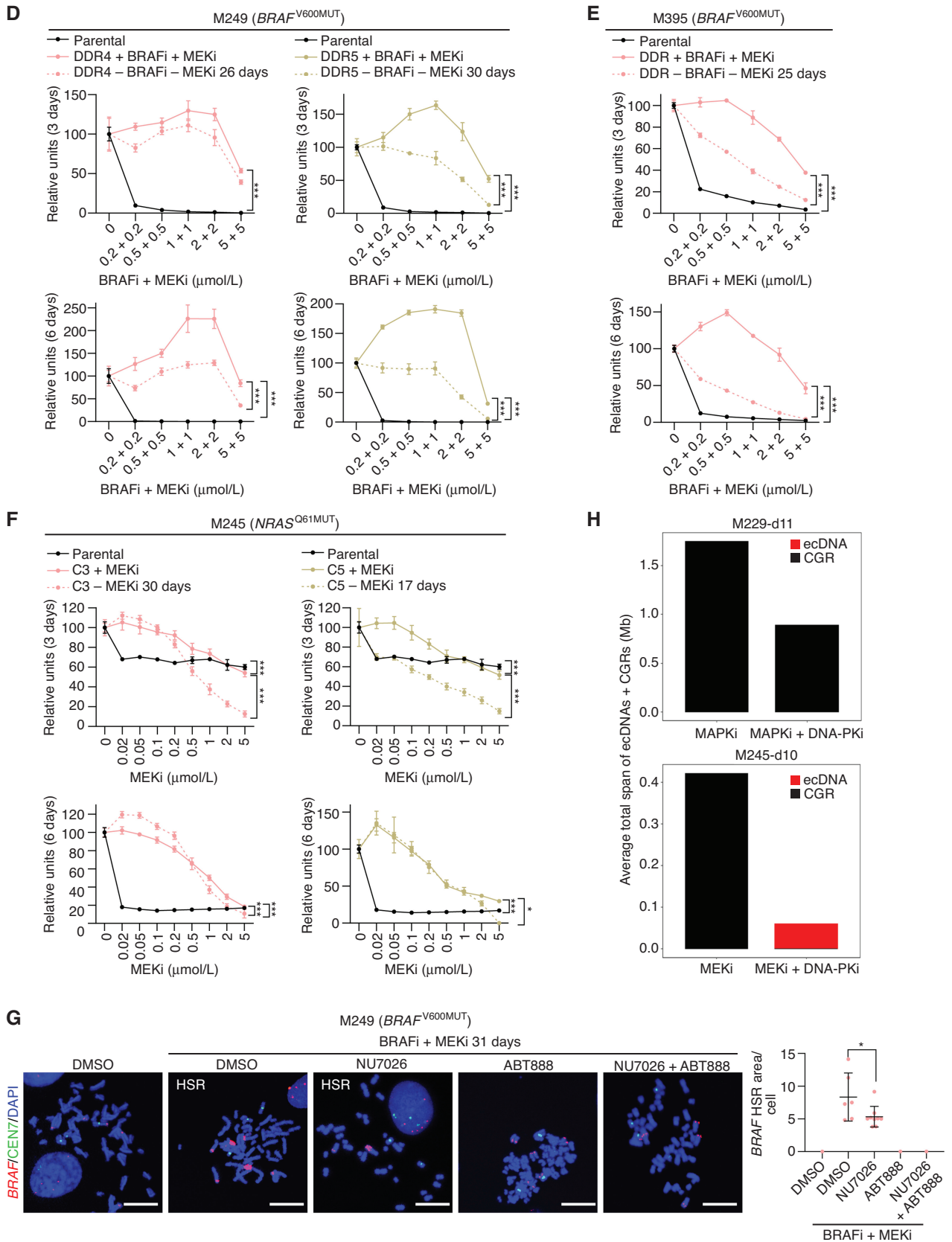
lines, without or with DNA-PKi and/or PARPi (Fig. 6). Interestingly, we observed that DNA-PKi effectively suppressed acquired MAPKi resistance in two of two *KRAS*[G12C] PDAC cell lines (Fig. 6A–F) and one of two *KRAS*[G12C] NSCLC cell lines (Fig. 6G–J). Moreover, PARPi was generally ineffective as a combinatorial agent with MAPKi. Future studies should explore the contributions of chromothripsis, ecDNAs, and CGRs to acquired MAPKi resistance in human *KRAS*[G12C] PDAC and NSCLC.

DNA-PKi Forestalls Resistance *In Vivo* and Reduces ecDNA and CGR Size

Given the broader resistance-preventive activity of DNA-PKi, we tested NU7026's *in vivo* efficacy in five cutaneous melanoma PDXs. In Mel_PDX16 (*BRAF*[V600MUT]) melanoma, using well-established tumors (~500–700 mm³; Fig. 7A), BRAFi + MEKi (vemurafenib at 90 mg/kg/d, trametinib at 0.7 mg/kg/d) elicited only tumor growth inhibition, and DNA-PKi treatment (8 mg/kg/d) had no discernible effect on tumor growth compared with vehicle-treated tumors. In contrast, the triplet of BRAFi + MEKi + DNA-PKi elicited tumor regression transiently for ~14 days until the tumors acquired resistance. There were no overt signs of toxicities or significant reductions in body weight in any experimental group. In Mel_PDX27 (*BRAF*[V600MUT]) melanoma (Fig. 7B; Supplementary Fig. S6A), BRAFi + MEKi (vemurafenib at 90 mg/kg/day, trametinib at 0.7 mg/kg/day) elicited transient tumor regression, whereas DNA-PKi treatment (8 mg/kg/day) did not elicit tumor regression compared with vehicle-treated tumors. In contrast, the triplet of BRAFi + MEKi + DNA-PKi significantly forestalled acquired

resistance, without incurring overt signs of toxicities or significant reductions in body weight. In *NRAS*[MUT] melanoma (Mel_PDX1; Fig. 7C), DNA-PKi treatment (10 mg/kg/d) did not elicit tumor regression, and MEKi (trametinib, 3 mg/kg/d) elicited only transient tumor regression. In contrast, the combination of MEKi + DNA-PKi led to minimally palpable tumors, without incurring toxicity. In two additional *NRAS*[MUT] melanoma PDXs (Mel_PDX2 and Mel_PDX4), we consistently observed superior efficacy of MEKi + DNA-PKi over MEKi alone (Fig. 7D and E). In Mel_PDX4, we initiated dosing with both DNA-PKi at 8 mg/kg/day and MEKi at 3 mg/kg/day but stopped dosing DNA-PKi (in combination with MEKi) on day 67 (Fig. 7E). With longer follow-up (Supplementary Fig. S6B), discontinuation of DNA-PKi dosing in this group of mice treated initially with MEKi + DNA-PKi did not lead to tumor relapse. Based on cell line findings (Fig. 4), we expected that delayed DNA-PKi cotreatment *in vivo* would also diminish its preventive mechanism of action. In Mel_PDX27 (*BRAF*[V600MUT]) melanoma (Fig. 7B; Supplementary Fig. S6A), we repeated BRAFi + MEKi (vemurafenib at 90 mg/kg/day, trametinib at 0.7 mg/kg/day) treatment, and, at the time of disease progression (when the mean tumor volume returned to the mean pre-MAPKi volume of ~500 mm³), we divided the tumors/mice into two groups. The first group continued on BRAFi + MEKi treatment at the same dosages, whereas the second group received DNA-PKi treatment (8 mg/kg/d) added on top of BRAFi + MEKi. Consistent with the cell line results (Fig. 4A–O), DNA-PKi cotreatment did not elicit discernible tumor regression on tumors that had already acquired MAPKi resistance *in vivo* (Fig. 7F).

Figure 5. Resistance-driver ecDNAs and HSRs dynamically track with resistance, and DNA-PKi prevents the size expansion of ecDNAs and CGRs early on MAPKi treatment. **A–C,** Metaphase DNA-FISH of paired parental and acquired resistant *BRAF*[V600MUT] (**A** and **B**) or *NRAS*[Q61MUT] (**C**) cell lines without or with drug withdrawal showing ecDNA or HSR amplicons harboring *BRAF*, *RAF1*, or *NRAS*. Left, representative images; right, quantifications per cell. Scale bars, 15 µm. *P* values (unpaired two-tailed Student *t* test): *, $P < 0.05$; **, $P < 0.01$; ***, $P < 0.001$. (*continued on next page*)

D M249 (*BRAF*^V600MUT)

E M395 (*BRAF*^V600MUT)

F M245 (*NRAS*^Q61MUT)

H

G M249 (*BRAF*^V600MUT)

BRAFi + MEKi 31 days

We then explored early on-treatment pharmacodynamic markers that are associated with the superiority of MAPKi + DNA-PKi over MAPKi alone in forestalling or preventing acquired resistance. We posited that the combination of DNA-PKi with MAPKi (versus MAPKi alone) would suppress the total size of ecDNAs and CGRs specifically generated due to MAPKi treatment, agnostic of content genes, regulatory elements, and known or putative roles in driving resistance. Using all five PDX models, we collected early on-treatment tumors and vehicle-treated tumors (Supplementary Fig. S6C and S6D). Expectedly, p-ERK was suppressed strongly in both groups of tumors treated with MAPKi or MAPKi + DNA-PKi (Supplementary Fig. S6E). Binding of the DNA-PK holoenzyme (DNA-PK$_{CS}$ + Ku70 + Ku80) to DSBs elicits autophosphorylation of DNA-PK$_{CS}$ on serine 2056. We found that DNA-PKi treatment, with or without MAPKi, suppressed nuclear p-DNA-PK$_{CS}$ foci (Supplementary Fig. S6F), which is consistent with NU7026 being able to suppress the kinase activity and autophosphorylation of the activated DNA-PK holoenzyme. We found that short-term MEKi treatment in Mel_PDX1 induced γH2AX nuclear foci in >50% of tumor cells (Supplementary Fig. S6G), consistent with a recent report that found MAPKi treatment resulting in γH2AX nuclear foci or DSBs in melanoma cell lines (42). Expectedly, DNA-PKi cotreatment with MEKi further induced DSBs marked by γH2AX foci. We then generated WGS data to enable an analysis of CGR and ecDNA amplicons (Supplementary Table S11). CGR and ecDNA amplicons identified in vehicle-treated PDX tumors were considered as background and were removed from those identified in MAPKi- or MAPKi + DNA-PKi–treated tumors. Consistent with our hypothesis, MAPKi + DNA-PKi (versus MAPKi) treatment was associated with reductions in the average total genomic spans of CGRs and ecDNAs in five of five PDX models analyzed (Fig. 7G). We also analyzed the break-point–junctional sequences of MAPKi treatment–specific ecDNAs and CGRs to infer the relative contributions of DSB repair pathways (Supplementary Fig. S6H). Consistent with the functional role of DNA-PKi, its combination with MAPKi suppressed the contribution of NHEJ, with potentially compensatory increases in alt-NHEJ or HRR processes.

DISCUSSION

Preexisting tumor heterogeneity and *de novo* diversification in response to targeted therapy are thought to fuel the evolution of acquired resistance. Here, we provide insights into the underlying genomic instability processes that generate preexisting and therapy-elicited clonal diversification in advanced cutaneous melanoma. We identified chromothripsis as well as ecDNAs and CGRs as highly recurrent and pervasive genomic SVs in MAPKi-naive/sensitive and acquired MAPKi-resistant melanoma in both the clinical setting (*BRAF*^{V600MUT} melanoma, in which MAPKi therapy is a standard-of-care therapy) and the experimental setting (*NRAS*^{MUT} melanoma, in which there is a lack of targeted therapy options). CGRs can derive from reintegration of ecDNAs or breakage–fusion–bridge (BFB) cycles (20, 43). We did not detect any BFB event in any of our tumors, MAPKi-sensitive/naive or acquired-resistant, favoring ecDNA reintegration as the main route of CGR generation in the setting of metastatic cutaneous melanoma. Consistently, the acute stress of MAPKi therapy favors ecDNAs, whereas stable or chronic stress favors reintegration of ecDNAs into chromosomes as HSRs (13). Moreover, following chromothripsis, chimeric circularization of DNA and reintegration of DNA circles into chromosomes constitute a major source of SVs and linear genome mutagenesis (44, 45). Importantly, the selective pressure of MAPKi therapy is evidenced by the amplification of bona fide resistance-driver genes via ecDNAs and CGRs. The report here of resistance-specific ecDNAs and CGRs amplifying a wide array of coding and noncoding sequences warrants future investigations into their resistance-causative mechanisms.

Even though chromothripsis is regarded as a potential precursor of ecDNAs, it creates oscillating CNs of genomic segments but does not cause high-level amplifications. We found that, within each tumor, ecDNAs (mean total size per genome, 7 Mb; mean size per ecDNA, 343 kb) and their reintegrated CGR counterparts (mean total size per genome, 6 Mb; mean size per CGR, 598 kb) almost always span genomic regions bounded by larger chromothriptic regions (mean total size per genome, 474 Mb; mean size per chromothriptic region, 120 Mb), which is consistent with a chromothriptic origin of ecDNA and CGR amplicons. Chromothripsis can occur as a result of micronuclei formation around lagging chromosomes or chromosome bridge formation due to telomere crisis (46–48). Both aberrant processes are associated with a loss of primary or micronuclear membrane integrity and subsequent mutagenesis. This is consistent with our finding of enhanced mutational density within chromothriptic genomic regions, especially within acquired-resistant genomes, as well as a resistance-specific mutator phenotype enriched for signatures of excessive single-stranded DNA damage and/or deficient repair (BER and MMR). Intriguingly,

---

Figure 5. *(Continued)* **D–F,** Three-day (top) and six-day (bottom) MTT assay of indicated cell lines treated with graded concentrations of BRAFi + MEKi (**D** and **E**) or MEKi (**F**). Cell viability was normalized to respective DMSO/vehicle groups. Inner brackets, comparisons between acquired resistant sublines without and with drug withdrawal. Outer brackets, comparisons between acquired resistant sublines and their isogenic parental cell lines. *P* values (two-way ANOVA test): *, *P* < 0.05; ***, *P* < 0.001. **G,** Representative images (left) and quantification (right) of metaphase DNA-FISH showing HSR harboring *BRAF* in M249 cells treated with vehicle or BRAFi + MEKi with or without NU7026 and/or ABT888 for 31 days. Inhibitor concentrations: BRAFi + MEKi (PLX4032 at 0.25 μmol/L, AZD6244 at 0.25 μmol/L), NU7026 (4 μmol/L), ABT888 (2 μmol/L), and NU7026 + ABT888 (4 μmol/L + 2 μmol/L). CEN, centromere; DAPI, nuclear stain. Scale bars, 15 μm. *P* values (unpaired two-tailed Student *t* test): *, *P* < 0.05. **H,** Average total genomic spans of treatment-specific ecDNAs + CGRs in M229 and M245 cell lines (background ecDNA + CGR spans detected in vehicle-treated cells were filtered). Inhibitor concentrations: BRAFi + MEKi (PLX4032 at 1 μmol/L, AZD6244 at 1 μmol/L for M229) or MEKi (trametinib at 0.02 μmol/L for M245), DNA-PKi (NU7026 at 8 μmol/L for both cell lines).
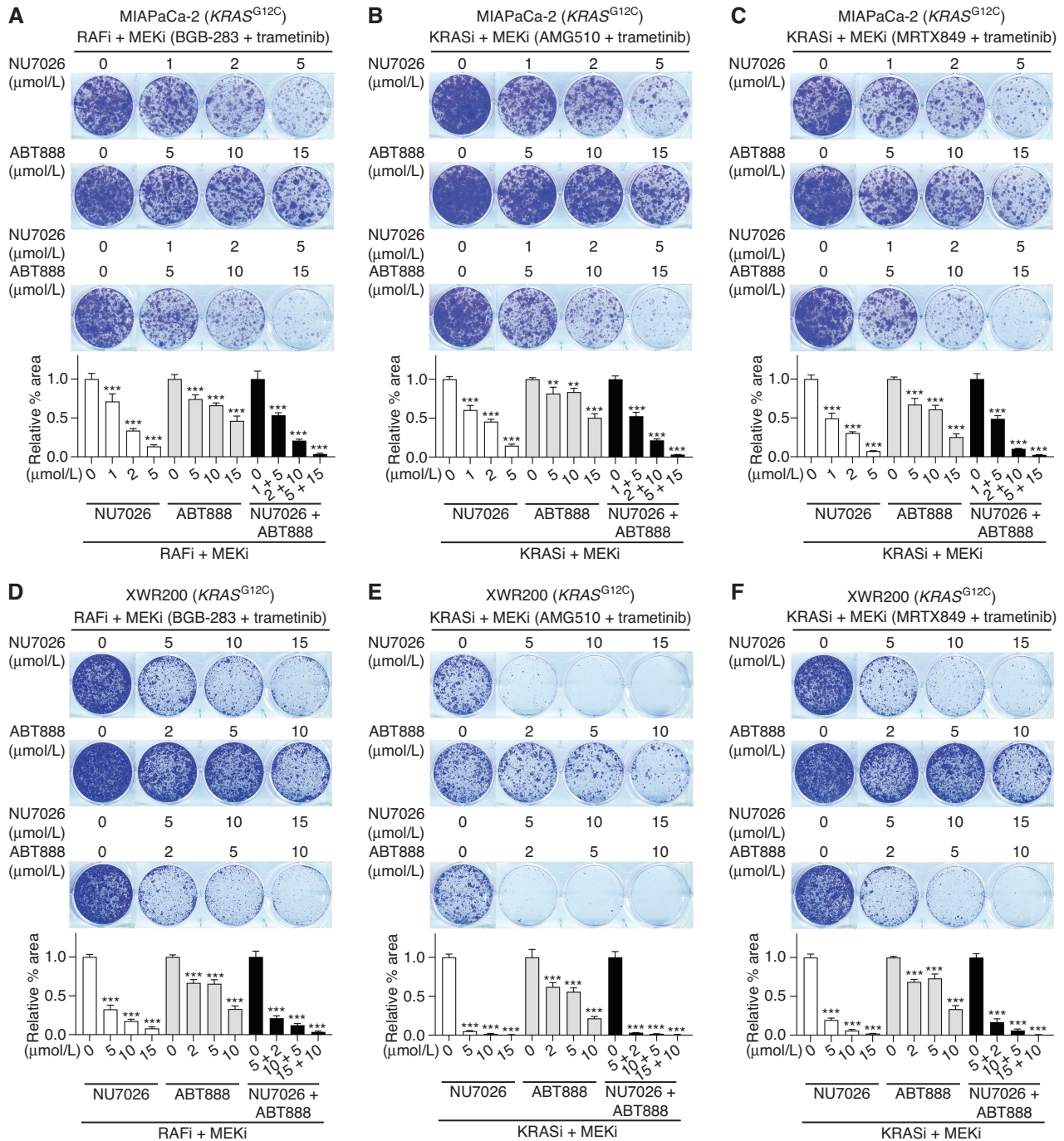
Figure 6. DNA-PKi cotreatment prevents acquired MAPKi resistance in *KRAS*[G12] human PDAC and NSCLC cell lines. **A–J,** Long-term clonogenic growth of PDAC (MIAPaCa-2, XWR200; **A–F**) or NSCLC (H358, H2122; **G–J**) cell lines showing acquired resistant colonies to MEKi alone, type II RAFi + MEKi, or KRAS[G12Ci] + MEKi and their suppression by indicated cotreatments with DNA-PKi (NU7026) and/or PARPi (ABT888) at indicated concentrations. Top, representative cultures; bottom, quantifications over *n* = 4 fields (mean ± SD). Data representative of 2 independent repeats. KRASi, KRAS inhibitor. Seeding densities (cells/well in 6-well dishes) and culture durations: MIAPaCa-2 (10,000; 30 days for **A–C**) and XWR200 (150,000; 23 days for **D**, 30 days for **E**, 26 days for **F**). (*continued on following page*)

a recent study proposed that a specific BER defect may predispose micronuclei-associated or cytoplasmic chromosomes to breakage, a key step toward chromothripsis (49).

Translationally, we produced *in vivo* evidence supportive of the well-studied role of DNA-PK_{CS} in NHEJ as critical

in promoting the total segment sizes of ecDNAs and CGRs generated early on MAPKi therapy. This finding is consistent with prior literature supporting NHEJ as key to ecDNA formation (28, 50). Selection for numeric expansion of specific ecDNAs and CGRs is considered a direct mechanism
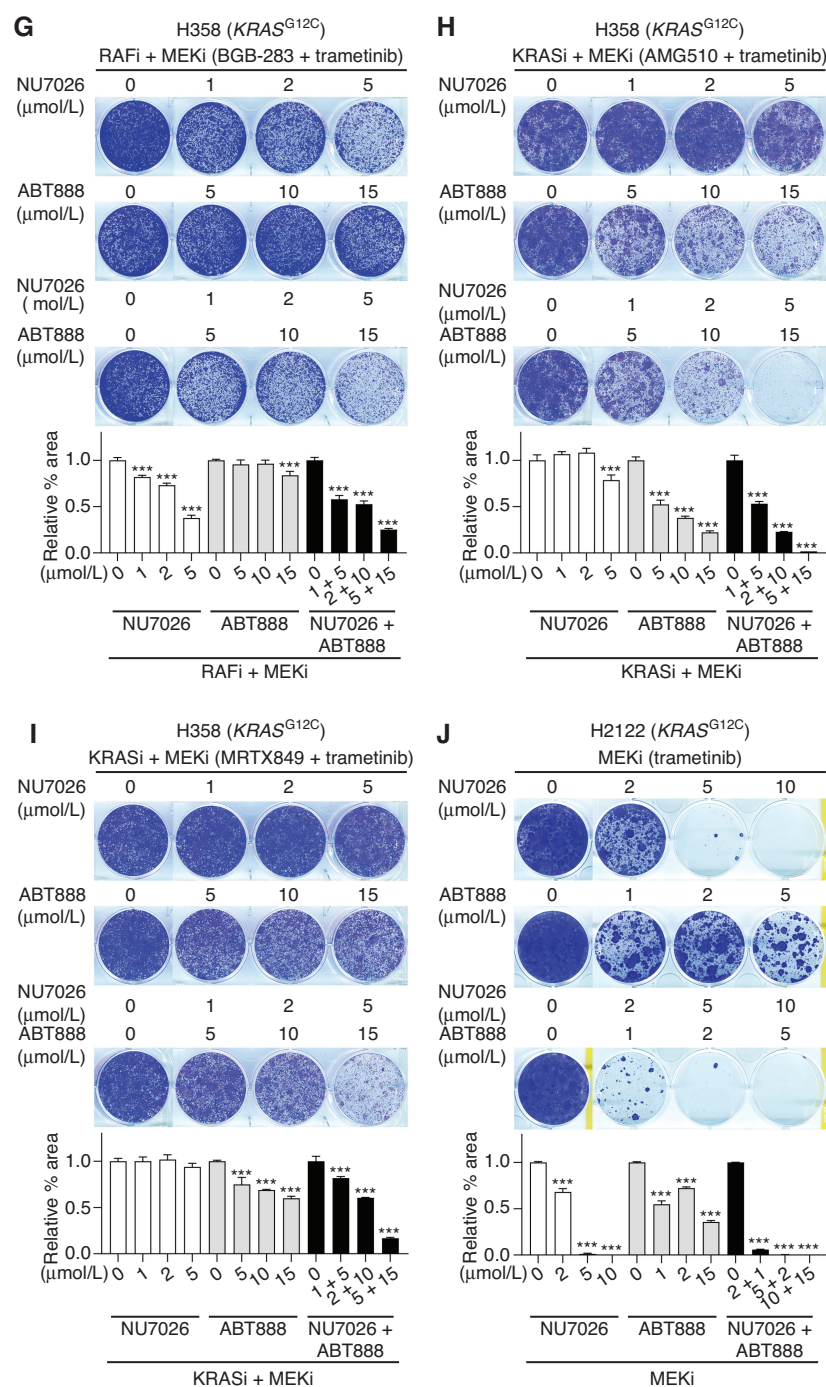
Figure 6. *(Continued)* Seeding densities (cells/well in 6-well dishes) and culture durations: H358 (40,000; 14 days for **G**, 29 days for **H**, 26 days for **I**) and H2122 (20,000, 22 days for **J**). Concentrations of type II RAFi (BGB-283) + MEKi (trametinib) or KRAS^{G12Ci} (AMG510 or MRTX849) + MEKi (trametinib) or MEKi (trametinib): 0.5 µmol/L + 0.01 µmol/L (**A**), 0.02 µmol/L + 0.01 µmol/L (**B**), 0.01 µmol/L + 0.01 µmol/L (**C**), 0.1 µmol/L + 0.001 µmol/L (**D**), 0.005 µmol/L + 0.001 µmol/L (**E**), 0.001 µmol/L + 0.001 µmol/L (**F**), 0.2 µmol/L + 0.001 µmol/L (**G**), 0.005 µmol/L + 0.001 µmol/L (**H**), 0.002 µmol/L + 0.001 µmol/L (**I**), and 0.02 µmol/L + 0.001 µmol/L (**J**). Data representative of 2 to 4 independent repeats. *P* values (one-way ANOVA followed by Tukey multiple comparisons test) comparing indicated cultures versus MAPKi treatment-only cultures: **, $P < 0.01$; ***, $P < 0.001$.

promoting tumor fitness in response to a given stressor. Therefore, reduction of the total ecDNA/CGR genomic spans early on DNA-PKi cotreatment should serve to reduce the reservoir of ecDNAs/CGRs available for natural selection by MAPKi therapy.

DNA-PK_{CS}, the target of DNA-PKi, subserves other less-characterized cancer survival pathways (37). It is possible that another beneficial mechanism of action of DNA-PKi coexists. DNA-PKi has been proposed in combination with agents that directly induce DNA damage, such as radiotherapy or chemotherapy, with the intent of radio- or chemosensitization (37). The rationale is based on catastrophic DSBs that would result in excessive DNA damage repair stress and hence the synergistic induction of death in cancer cells, especially those overexpressing DNA-PK_{CS}. Here, we rationalize the combination of DNA-PKi and MAPKi based on dual concepts. First, the rapid induction of genomic instability mechanisms, in particular the generation of ecDNA and CGR amplicons, is critical for genomic diversification and perhaps epigenomic reprogramming necessary for melanomas to adapt quickly to MAPKi therapy. In this rationale, DNA-PKi suppresses
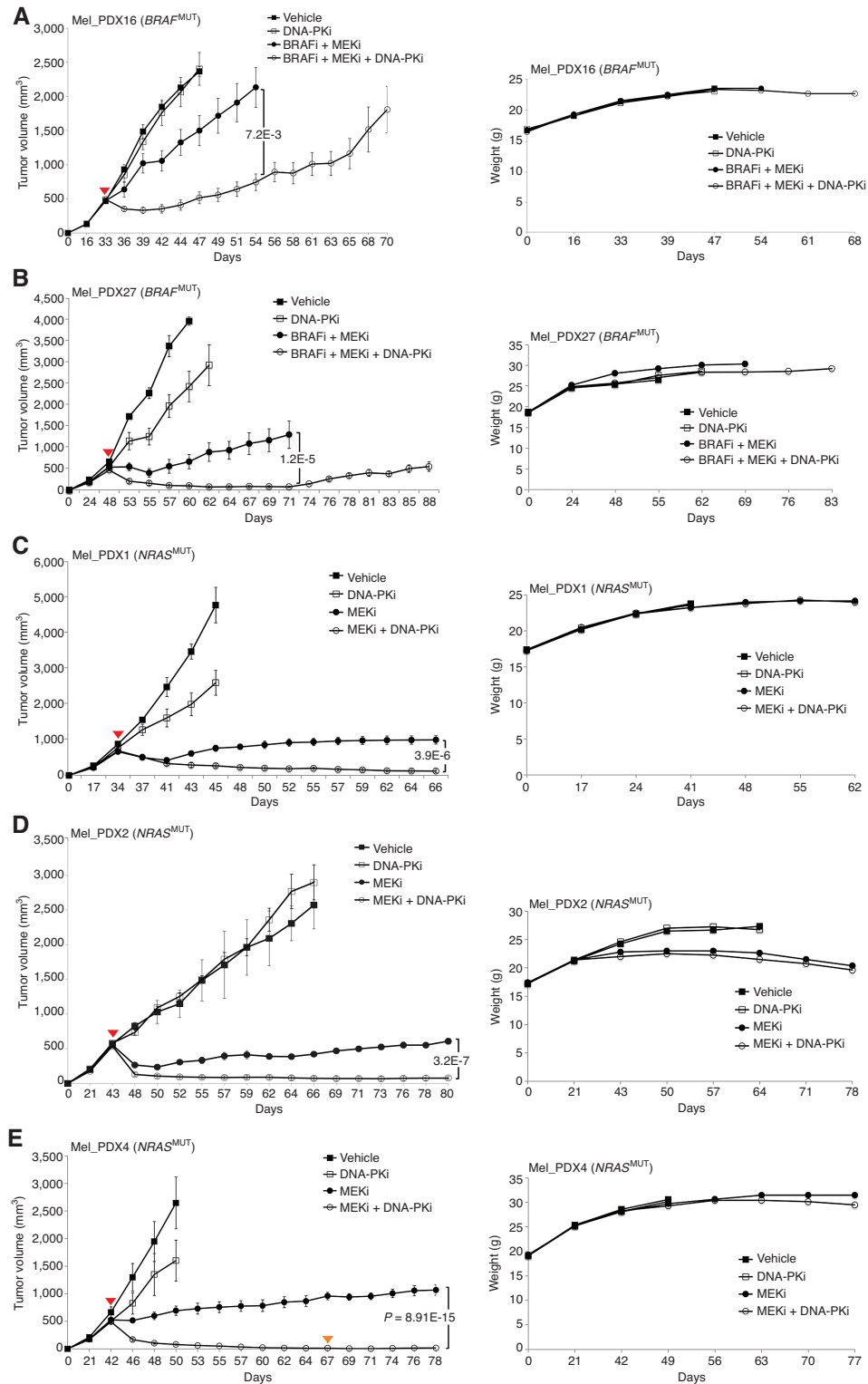
Figure 7. DNA-PKi cotreatment with MAPKi reduces the size of ecDNAs and CGRs and prevents acquired resistance *in vivo*. **A–E,** Measurements of tumor volumes (left) and body weights of mice (right) in two *BRAF*[V600MUT] (**A** and **B**) and three *NRAS*[MUT] (**C–E**) cutaneous melanoma PDX models. Vehicle or indicated treatments initiated on well-established tumors on days 33 (**A**), 48 (**B**), 34 (**C**), 43 (**D**), and 42 (**E**) after tumor fragment implantation, as marked by upside-down red triangles. Dosage of inhibitors DNA-PKi (NU7026), BRAFi (vemurafenib), and MEKi (trametinib; mg/kg/day): DNA-PKi, 8; BRAFi, 90; MEKi, 0.7 (**A** and **B**); DNA-PKi, 10; MEKi, 3 (**C**); DNA-PKi, 6; MEKi, 5 (**D**); and DNA-PKi, 8 (stopped on day 67 when in combination with MEKi, as marked by an upside-down orange triangle); MEKi, 3 (**E**). One tumor per mouse; number of mice per experimental group (from top to bottom): 5, 5, 7, 7 (**A**); 4, 5, 8, 8 (**B**); 5, 5, 8, 5 (**C**); 3, 4, 8, 8 (**D**); and 5, 5, 6, 9 (**E**). Results are shown as mean ± SEM. *P* values, Student *t* test. Body weights are shown as average values. (*continued on following page*)
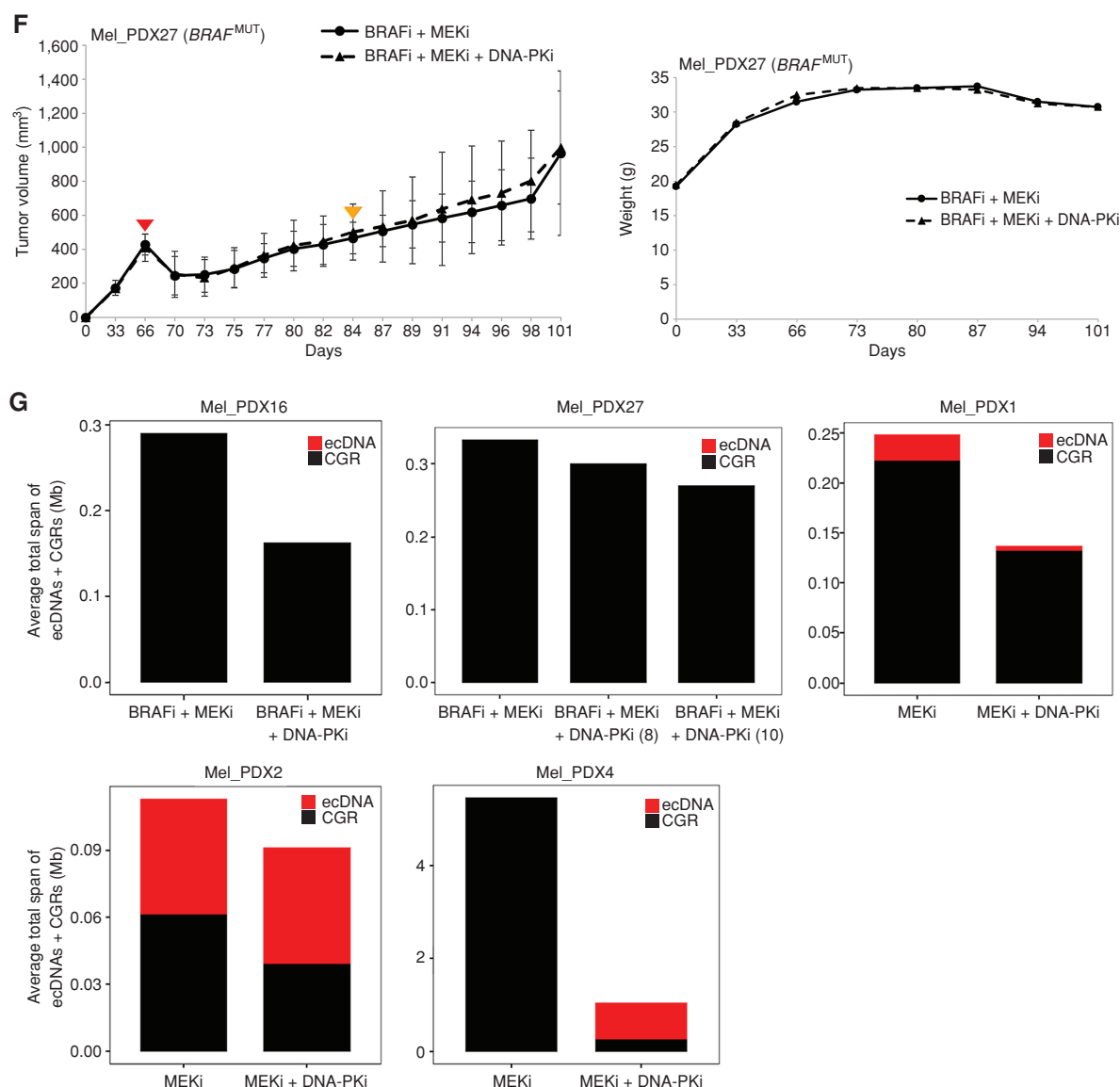
Figure 7. *(Continued)* **F,** As in Fig. 5B (BRAFi + MEKi treatment group), except at the earliest time of acquired resistance (day 84, marked by an upside-down orange triangle), tumors or mice were divided into two groups (*n* = 5 each). Group 1 continued on BRAFi + MEKi treatments. Group 2 received DNA-PKi (8 mg/kg/day) in combination with BRAFi + MEKi treatments. **G,** Average total spans of ecDNAs + CGRs specific to MEKi-treated versus MEKi + DNA-PKi–treated PDXs (background ecDNAs + CGRs detected in vehicle-treated tumors were filtered) in Mel_PDX16 (BRAFi + MEKi–treated, *n* = 3; BRAFi + MEKi + DNA-PKi–treated, *n* = 3), Mel_PDX27 (BRAFi + MEKi–treated, *n* = 3; BRAFi + MEKi + DNA-PKi (8 mg/kg/day)–treated, *n* = 3; BRAFi + MEKi + DNA-PKi (10 mg/kg/day)–treated, *n* = 2), Mel_PDX1 (MEKi-treated, *n* = 2; MEKi + DNA-PKi–treated, *n* = 2), Mel_PDX2 (MEKi-treated, *n* = 2; MEKi + DNA-PKi–treated, *n* = 2), and Mel_PDX4 (MEKi-treated, *n* = 2; MEKi + DNA-PKi–treated, *n* = 3). Tumors were collected for analysis on days 6 (Mel_PDX16), 7 (Mel_PDX27), 11 (Mel_PDX1), 9 (Mel_PDX2), and 8 (Mel_PDX4) after initiating treatments.

NHEJ, which is necessary for the efficient formation of ecDNAs and CGRs. Second, MAPKi is potentially an inducer of DNA damage and/or DNA damage repair deficiency. In this context, MAPKi has been shown to induce DNA damage in early drug-tolerant persister subpopulations (42). A therapy-induced oxidative metabolic adaptation (51) has been proposed to cause ROS-induced mutagenesis, which can be repaired by DNA single-stranded break (SSB) repair processes such as BER and MMR. DNA-PK$_{CS}$, in addition to DSB repair, can also bind to and is activated by DNA SSBs

(52). Excessive DNA SSBs can be converted into DNA DSBs, engendering DNA damage repair stress and/or chromosome breakage. The latter may be a pathway to chromothripsis and ecDNA/CGR generation (49).

Our demonstration of ecDNAs and CGRs driving acquired MAPKi resistance advances the concept that multiple resistance mechanisms, genetic and epigenetic, as well as direct (drug–target or MAPK pathway reactivation) and indirect (nondrug–target pathway activation), are simultaneously causal of clinically acquired resistance. Future work needs to

dissect this hybrid genomic–epigenomic model with ecDNAs and CGRs at the center of therapeutic targeting efforts. Findings here also advance the concepts that preventing, instead of reversing, acquired resistant phenotypes may be more impactful clinically and that targeting DNA-PK$_{CS}$ and NHEJ, and potentially MMEJ and HRR, lies at the center of this approach in stabilizing cancer genomes during oncogene-targeted therapies. Finally, prevention of chromothripsis, such as by reducing chromosome fusion and missegregation events and minimizing primary and micronuclei membrane ruptures, may expand our molecular armamentarium against targeted therapy resistance.

METHODS

Human Subjects

Patient characteristics related to clinical tissues are presented in Supplementary Table S1. Patient-derived tissues were obtained with written informed consent and approval by local institutional review boards.

Mice

NSG (NOD scid gamma) mice were obtained from the Radiation Oncology breeding colony at University of California, Los Angeles (UCLA). Male or female mice were used at 4 to 6 weeks of age. All animal experiments were conducted according to the guidelines approved by the UCLA Animal Research Committee.

PDX Models and In Vivo Treatments

To develop PDX models, tumor fragments derived from metastatic melanoma, with approval by the local institutional review boards, were transplanted subcutaneously in sex-matched NSG mice (4–6 weeks old). One tumor fragment was implanted in each mouse. Tumors were measured with a caliper every 2 days, and tumor volumes were calculated using the formula (length × width²)/2. Tumors with volumes around 500 mm³ were randomly assigned into experimental groups. Special mouse diets were generated to reduce stress to animals by incorporating trametinib (LC Laboratories) into chow to achieve daily trametinib dosing at 3 or 5 mg/kg/day or combined vemurafenib (LC Laboratories) and trametinib dosing at 90 mg/kg/day and 0.7 mg/kg/day, respectively (Test Diet). DNA-PKi (NU7026, Selleckchem) was dissolved in saline (UCLA Division of Laboratory Animal Medicine pharmacy) and administered intraperitoneally at 6, 8, or 10 mg/kg/day. We derived model- or patient-matched vehicle-treated tumors and acquired trametinib-resistant tumors as plotted in Supplementary Fig. S1A. We also derived model-matched vehicle-treated tumors and early on-treatment tumors as plotted in Supplementary Fig. S6C and S6D.

WGS

gDNA and total RNA were extracted from frozen tumor tissue preserved in RNALater or snap-frozen tumor tissue using the Qiagen AllPrep DNA/RNA Mini Kit and the Ambion mirVana miRNA Isolation Kit. Normal gDNA from peripheral blood mononuclear cells (PBMC) were extracted from fresh or frozen PBMCs using the Qiagen FlexiGene DNA Kit. All gDNA were quantified using a NanoDrop (Thermo Fisher Scientific) and Qubit fluorometer using the dsDNA BR Assay (Life Technologies), and then gDNA size and quality were tested using TapeStation (Agilent) to ensure gDNA libraries were prepared using equal gDNA input and presence of a high-molecular-weight band. Whole-genome libraries were prepared using the Roche KAPA HyperPrep Kit. Briefly, after enzymatic fragmentation of gDNA, the libraries were constructed by end repairing and A-tailing the fragmented DNAs, ligation of adapters, and PCR amplification. After library construction, indexed libraries were quantified for equal molar pooling and paired-end sequenced with a read length of 2 × 150 bp on the Illumina NovaSeq 6000 S4 platform.

Whole-genome libraries were prepared for patient-matched normal tissues and tumors as follows: (i) 10 $BRAF^{V600MUT}$ clinical patients (baseline tumors, $n = 10$; resistant tumors, $n = 17$), (ii) three $BRAF^{MUT}$ RAM patients (sensitive tumor, $n = 1$; resistant tumors, $n = 12$), and (iii) six PDX models. PDX models included one $BRAF^{MUT}$ PDX (vehicle-treated tumor, $n = 1$; resistant tumors $n = 3$) and five $NRAS^{MUT}$ PDXs (vehicle-treated tumors, $n = 5$; resistant tumors, $n = 9$). For early on-treatment samples, we prepared whole-genome libraries from (i) one human $BRAF^{V600MUT}$ (M229; DMSO, $n = 1$; BRAFi + MEKi, $n = 1$; BRAFi + MEKi + DNA-PKi, $n = 1$) and one $NRAS^{MUT}$ (M245; DMSO, $n = 1$; MEKi, $n = 1$; MEKi + DNA-PKi, $n = 1$) cutaneous melanoma cell line and (ii) two $BRAF^{V600MUT}$ (vehicle, $n = 6$; BRAFi + MEKi, $n = 6$; BRAFi + MEKi + DNA-PKi, $n = 9$) and three $NRAS^{MUT}$ (vehicle, $n = 6$; MEKi, $n = 6$; MEKi + DNA-PKi, $n = 7$) cutaneous melanoma PDX models. Also, whole-genome libraries were prepared for vehicle-treated tumors and early on-treatment tumors from two $NRAS^{MUT}$ PDX models. In total, paired-end sequencing was performed on 123 (104 tumors or cell lines, 19 patient-matched normal tissues) genomes using Illumina NovaSeq S4 with a read length of 2 × 150 bp and at a sequencing depth of 11 to 98× (median, 26×).

WGS Data Analysis

WGS reads were mapped to the GRCh38/hg38 human reference genome using BWA-MEM (53). Alignments were sorted, and PCR duplicates were removed using Samtools (54). CN variations were called using two depth-of-coverage–based methods CNVkit (55) and ReadDepth (56). Default parameters were used for CNVkit. We used an FDR of 0.05 and overdispersion of 1 for ReadDepth analysis. Structural variations reported by at least two SV detection methods: SvABA (57), TIDDIT (58), and DELLY (59) were considered. SVs in both DELLY and TIDDIT are determined by combining discordant read pairs and split-reads, whereas TIDDIT additionally uses depth-of-coverage signatures. SvABA utilizes discordant reads and genome-wide local assembly strategies for predicting SVs from the genome. For high-coverage data (>15×), default parameters were considered for SvABA, TIDDIT, and DELLY. Parameter minimum number of points (-l) was set to 5 in TIDDIT for low-coverage data.

Analysis of ecDNAs and CGRs

We carried out reconstruction of focal gene amplifications and elucidation of ecDNA and CGRs using AmpliconArchitect (60). Briefly, AmpliconArchitect determines the list of potential intervals for each amplicon to be reconstructed, and within each amplicon, CNs and SVs are estimated using read depth and discordant read signatures. It then constructs breakpoint graphs detailing sequence edges and breakpoint edges, and predicts copy counts of all edges. Simple cycles are then decomposed from the breakpoint graphs. Finally, AmpliconClassifier classifies the amplicons into ecDNAs, CGRs, and linear amplicons. Amplicons are classified as ecDNAs if the segment(s) forms a head-to-tail structure, with size >10 kb, and CN >4.5; as complex genomic rearrangements for noncircular amplicons containing DNA segments from different chromosomes or regions that are far apart (>1 Mb) on chromosomes; or as linear amplicons for linear amplifications. In our study, the initial set of CNV seed regions was inferred by ReadDepth and CNVKit. SV view of amplicons and circle plots of simple cycles were generated using functions available in AmpliconArchitect.

We carried out pathway enrichment analysis of genes within ecDNAs and/or CGRs using the Molecular Signatures Database with pathways listed in Gene Ontology, Kyoto Encyclopedia of Genes and Genomes, Reactome, and Pathway Interaction Databases. For each tumor sample, we identified somatic SNVs using Strelka2 (61) with default parameters. Next, we estimated SBS signatures in regions within and without ecDNAs and CGRs using the nonnegative matrix factorization–based tool MutationalPatterns (62) with COSMIC SBS signatures V3.3 as reference. We carried out mutational signature analysis using SNVs in ecDNAs and/or CGR regions of (i) acquired MAPKi-resistant (mutations in patient-matched sensitive tumors subtracted from mutations in resistant tumors) and (ii) MAPKi-sensitive genomes. To characterize whether SBS mutational signatures are preferentially detected within (versus outside of) ecDNAs and/or CGRs amplicons, we calculated the ratios of the proportions of signatures within ecDNA and/or CGR sequences and the proportion of signatures outside ecDNAs and/or CGR sequences and defined these ratios as SBS mutational signature enrichment score. We considered an enrichment score of 1 as the cutoff threshold. Scores >1 indicate SBS signatures enriched within ecDNAs and/or CGRs, whereas scores <1 indicate SBS signatures enriched in the background (non-ecDNA– and/or non-CGR–involved genomic regions). For clarity, only scores >1 and <1 were plotted.

We extracted enhancer elements and their connected genes from GeneHancer (version4-4, GeneCards). Genehancer is an integrated database of human enhancers and their inferred target genes, mined from four different genome-wide databases: ENCODE, FANTOM, the VISTA enhancer browser, and the Ensembl regulatory build. The enhancer–target genes associations were obtained from eQTLs, CHi-C, eRNA coexpression, transcription factor coexpression, and gene–enhancer distance methods. Annotations of superenhancers were obtained from dbSUPER (63). Enhancers were first assessed for their presence on CGR and ecDNA amplicons, and, if so, their connected oncogenes were searched for their presence within CGR/ecDNA amplicons (*cis* interaction) or elsewhere in the chromosome (*trans* interaction). Furthermore, we obtained H3K27 acetylation peaks from seven cell lines (GM12878, H1-hESC, HSMM, HUVEC, K562, NHEK, and NHLF) listed in ENCODE. The peaks aligned to ecDNA regions in Pt9-DD-DP2 (*MYC*) and Mel_PDX27-R2 (*BRAF*) were obtained from the UCSC Genome Browser.

Metaphase Chromosome Spread

Cells in metaphase were prepared by colcemid (Sigma) treatment at 10 μg/mL for several hours (depending on the growth rate). The single-cell suspensions were collected, washed with PBS, and then treated with 0.075 M KCl (Gibco) for 15 minutes. We then fixed and washed cells with 3:1 methanol:acetic acid. The final cell pellet was resuspended with the fixative and dropped onto a humidified slide.

DNA-FISH

Formalin-fixed, paraffin-embedded (FFPE) tissue samples were baked at 90°C for 25 minutes in an oven and immersed in 100% xylene and then 100% ethanol, each for 10 minutes to deparaffinize tissues. Air-dried tumor tissues were pretreated in 90°C to 95°C 10 mmol/L in citric acid buffer (pH 6.8, Thermo Fisher Scientific, 327162500) for 30 minutes and washed in 2× SSC buffer (Invitrogen, 15557044) for 5 minutes. Then, FFPE slides were digested in 37°C pepsin solution (Thermo Fisher Scientific, J6167906) for 20 to 30 minutes, washed in 2× SSC buffer for 5 minutes, and dehydrated in ascending ethanol series (70%, 85%, and 100%), each for 2 minutes. For metaphase DNA-FISH, fixed cells in interphase or metaphase on slides were dehydrated in ascending ethanol series (70%, 85%, and 100%), each for 2 minutes. We used the following DNA-FISH probes: *NRAS*/CEN1 amplification probe (NRAS-CHR01-20-ORGR) targeting *NRAS* or

centromeric region of chr1; *BRAF*/CEN7 amplification probe (BRAF-CHR07-20-ORGR) targeting *BRAF* or centromeric region of chr7; and *RAF1*/CEN3 amplification probe (RAF1-CHR03-20-ORGR) targeting *RAF1* or centromeric region of chr3, all from Empire Genomics. The probes were mixed with the provided hybridization buffer in a 1:4 ratio and applied onto the tissues or cells. FFPE samples were then denatured at 75°C in a slide moat for 7 minutes, whereas metaphase samples were denatured at 73°C for 2 minutes. We then performed hybridization overnight at 37°C in a humidified chamber. The samples were then washed at 73°C with 0.3% Igepal/0.4× SSC for 2 minutes, followed by another 2-minute wash with 0.1% Igepal/2× SSC at room temperature. Finally, the tissue samples were stained with ProLong Diamond Antifade Mountant with DAPI (Invitrogen, P36966) and covered by coverslips. Images were acquired on a Leica Confocal SP8-STED/FLIM/FCS microscope. For ecDNA quantification, we counted the number of specific gene foci in each nucleus by ImageJ (version, 1.52a). For HSR quantification, we counted the area of gene foci larger than 2 μm^2 to exclude ecDNA and non-HSR gene foci in each nucleus by ImageJ (version, 1.52a).

RNA-seq Analysis

Total RNAs were extracted from frozen tumor tissue preserved in RNALater of snap-frozen tumor tissues using the Qiagen AllPrep DNA/RNA Mini Kit and the Ambion mirVana miRNA Isolation Kit. Total RNAs were quantified by the Qubit RNA High Sensitivity kit (Thermo Fisher Scientific) and/or using a NanoDrop (Thermo Fisher Scientific). RNA size and quality were measured using an Agilent 2100 Bioanalyzer (Agilent Technologies). RNA libraries were constructed using the NuGen Universal Plus mRNA-Seq Kit. Briefly, after fragmentation of total RNA and double-stranded cDNA generation using a mixture of random and oligo(dT) primers, the RNA libraries were constructed by end repairing, adapter ligation, strand selection, and PCR amplification. Libraries were quantified for equal molar pooling and paired-end sequenced with a read length of 2×50 bp on the Illumina NovaSeq 6000 S4 platform.

We mapped paired-end reads of patient-matched tumor samples from 10 patients and 6 PDX models to the GRChr38 human reference genome using STAR aligner (64) with default parameters. Log$_2$ fold change values were calculated for each acquired resistant tumor compared with patient- or model-matched pretreatment tumor or vehicle-treated tumor, respectively. Genes with an absolute fold change >2 were considered significant. Gene counts were estimated using FeatureCounts (65) with GENCODE (version 38) annotations. Feature counts were then normalized using trimmed mean of M values (TMM) approach and log$_2$ transformed (66). Fold changes for each gene were estimated by computing the difference between the normalized values of acquired resistant tumors and MAPKi-sensitive/naive transcriptomes.

Analysis of Chromothripsis

To infer chromothriptic events in the genomes, we applied ShatterSeek (12), an *in silico* scoring algorithm based on the clusters of interleaved SVs, CN oscillations, and interchromosomal SVs. CN and SVs described above were considered as input for ShatterSeek. High-confidence chromothriptic events were selected based on the statistical criteria recommended by the authors. Briefly, a high-confidence chromothriptic event is characterized with (i) a cluster of SVs (>6 DUP/DEL/h2hINV/t2tINV), (ii) oscillating CN between two states (>7 CN events), (iii) chromosomal enrichment and distribution of DNA breakpoints ($P < 0.05$), (iv) randomness of fragment joins ($P > 0.05$), and/or (v) interchromosomal rearrangements between multiple chromosomes. Somatic SNVs spanning chromothripsis regions were identified using Strelka2 (61) with default parameters and defined as chromothripsis-associated SNVs. Regions with and without chromothripsis were extracted and TMBs were computed

within these regions for each tumor sample. Ratios between TMBs within and outside of chromothriptic regions were calculated. Mutational signature analysis was carried out using SNVs in chromothriptic regions of (i) acquired MAPKi-resistant (mutations in patient-matched sensitive tumors subtracted from mutations in resistant tumors) and (ii) MAPKI-sensitive genomes. Mutational (SBS, DBS, and ID) signatures for each sample were predicted using nonnegative matrix factorization–based tool MutationalPatterns (62), and the extracted signatures were compared with the COSMIC SBS, DBS, and ID signature database.

Junctional Sequence Analysis of Amplicon Breakpoints

Sequences of CGRs and ecDNAs identified in all the genomes were analyzed. Breakpoints of amplicons harboring key MAPKi-resistance genes, *BRAF*, *NRAS*, *HRAS*, and *EGFR*, were extracted, and sequences spanning these junctions were further analyzed. Homologous sequences and insertions for the breakpoint junctions were obtained from SvABA, and a possible mechanism for DNA DSB repair was inferred. First, HRR was identified with large homologous sequences and insertions (≥8 bp). Second, MMEJ or alt-NHEJ was identified with breakpoints comprising homologous sequences (2–8 bp). Third, NHEJ was identified when neither of the sequence types described above was identified in the vicinity of the breakpoints.

Cell Lines and Inhibitor Treatments

All cell lines were routinely tested for *Mycoplasma* and profiled and identified by RNA-seq and the GenePrint 10 system (Promega) at periodic intervals during the course of this study. All M series cell lines were established from patient-derived tumors at the UCLA with institutional review board approval. All M cell lines with acquired MAPKi resistance were derived in the Lo Laboratory and published previously (3, 5, 8, 9, 11, 22, 40, 67). We maintained H358 (ATCC) in RPMI 1640 (Gibco) with 10% heat-inactivated FBS (Omega Scientific, FB-02) and 2 mmol/L glutamine in a humidified, 5% CO_2 incubator at 37°C; all other cell lines were maintained in high-glucose DMEM (Omega Scientific, DM-22) with 10% heat-inactivated FBS (Omega Scientific, FB-02) and 2 mmol/L glutamine in a humidified, 5% CO_2 incubator at 37°C. We obtained inhibitors from the following sources: PLX4032 (Plexxikon), AZD6244 (Selleck Chemicals), trametinib (LC Laboratories), NU7026 (Abcam, ab120970), ABT888 (Enzo, ALX-270-444-M005), VX984 (MCE, HY-19939S), AZD7648 (TargetMol, T7122), olaparib (LC Laboratories, 763113-22–0), MRTX849 (Selleckchem, S8884), AMG510 (Selleckchem, S8830), and BGB-283 (BeiGene, via a Material Transfer Agreement with UCLA). All inhibitors were dissolved in DMSO and stored at −20°C.

Lentivirus Production, Transduction, and shRNA Sequences

shRNAs for *PRKDC* and vector control (pGIPZ) were obtained from Robert Damoiseaux, PhD (Molecular Screening Shared Resource, UCLA); shRNAs for *LIG4* were from Sigma. All shRNAs were packaged into lentiviral particles for infection. The lentiviral viruses were generated by transfection of the constructs together with pMD2.G, pRSV-Rev, and pMDLg/pRRE into HEK-293T cells using calcium phosphate. Fourteen hours after transfection, media were replaced with preheated fresh media. Virus particles were harvested 24 and 48 hours later and filtered by a 0.45 μm filter unit (Millipore). Cells were transduced with recombinant lentivirus with 10 μg/mL polybrene (Millipore, TR-1003-G) for 48 hours and then selected by puromycin (Sigma, P8833) for 1 week. shRNA targeting sequences were as follows:

Human *PRKDC* sh1: CAGTGAAAGTCTGAATCAT
Human *PRKDC* sh2: GTCATGGATTCAAGAAATA
Human *PRKDC* sh3: GAGCTTACATGCTAATGTA

Human *PRKDC* sh4: GGTCATGGATTCAAGAAAT
Human *LIG4* sh1: TTCGACGCCACACCGTTTATT
Human *LIG4* sh2: TATGTCAGTGGACTAATGGAT

Cell Growth Assays

For clonogenic assay, cells were plated at indicated cell densities in 6-well plates and treated with inhibitor(s) the next day. Inhibitors and media were replenished every 2 days for the number of days indicated. Colonies were fixed in 4% paraformaldehyde, followed by staining with 0.1% crystal violet. For the MTT assay, cells were plated at 2,000 cells per well in 96-well plates (Fig. 4P and Q); parental and acquired resistant sublines were seeded at 4,000 cells per well and treated with graded concentrations of MAPKi the next day (Fig. 5D–F); and media were replenished every 2 to 3 days. Methylthiazolyldiphenyl-tetrazolium bromide (MTT; 100 μL) solution (0.5 mg/mL, Sigma, M5655) was added to each well and incubated at 37°C for 2 hours for MTT formazan formation. Formazan was then dissolved in 100 μL DMSO, and the absorbance values were measured using an ELISA reader (SpectraMax Plus 384) at the wavelength of 570 nm, blanked with DMSO solution. Experiments were performed with 4 replicates.

Western Blots

Cells were lysed in RIPA buffer (Thermo Fisher Scientific) with protease inhibitor cocktail (Thermo Fisher Scientific) and phosphatase inhibitor cocktails (Thermo Fisher Scientific) for Western blotting. BCA protein assay (Thermo Fisher Scientific, PI23227) was used to determine the protein concentration. Antibodies used in Western blot were as follows: TUBULIN (Cell Signaling Technology, 2144S), PRKDC (Cell Signaling Technology, 38168S), and LIG4 (Cell Signaling Technology, 14649S).

Immunofluorescence Analysis

Tumor tissues were fixed in formalin followed by paraffin embedding. After deparaffinization and rehydration, tissue sections were antigen retrieved by heat. Permeabilization and blocking were followed by overnight incubation with primary antibodies [p-ERK1/2 (Cell Signaling Technology, 4370), p-DNA-PKcs (Abcam, ab124918), p-H2AX (Cell Signaling Technology, 9718)]. Immunofluorescence was performed with Alexa Fluor–conjugated secondary antibodies (Life Technologies, A-21429). Nuclei were counterstained by DAPI. Signals were captured with a Zeiss microscope (AXIO Imager A1) mounted with a charge-coupled device camera (Retiga EXi QImaging), and images were captured by Image-Pro plus 6.0.

Statistical Methods

Statistical analysis for genomic data was conducted in R.4.02, Python 3.8.0, and Python 2.7.17. Statistical analyses, described for specific experiments, for cell line– or PDX tumor–based assays were performed using GraphPad Prism.

Data Availability

The BAM files of WGS data are deposited in the European Genome-phenome Archive (https://www.ebi.ac.uk/ega/) with the accession number EGAS00001006874. This study did not generate custom codes. Any additional information regarding data reported in this article is available from the corresponding author upon request. There are no restrictions on data availability.

Authors' Disclosures

A. Ribas reports personal fees (honoraria) from Amgen, Bristol Myers Squib, Chugai, Genentech, Merck, Novartis, Roche, Sanofi,

Authors' Contributions

P. Dharanipragada: Data curation, formal analysis, investigation, visualization, methodology, writing–original draft, writing–review and editing. **X. Zhang:** Formal analysis, investigation, visualization, methodology, writing–review and editing. **S. Liu:** Data curation, formal analysis, methodology, writing–review and editing. **S.H. Lomeli:** Resources, methodology, writing–review and editing. **A. Hong:** Formal analysis, visualization, methodology, writing–review and editing. **Y. Wang:** Methodology, writing–review and editing. **Z. Yang:** Resources, methodology, writing–review and editing. **K.Z. Lo:** Resources, methodology. **A. Vega-Crespo:** Resources. **A. Ribas:** Resources. **S.J. Moschos:** Resources, methodology, writing–review and editing. **G. Moriceau:** Resources, formal analysis, visualization, methodology, writing–review and editing. **R.S. Lo:** Conceptualization, resources, data curation, formal analysis, supervision, funding acquisition, validation, investigation, visualization, methodology, writing–original draft, project administration, writing–review and editing.

Acknowledgments

Note

REFERENCES

1. Flaherty KT, Puzanov I, Kim KB, Ribas A, McArthur GA, Sosman JA, et al. Inhibition of mutated, activated BRAF in metastatic melanoma. N Engl J Med 2010;363:809–19.
2. Flaherty KT, Infante JR, Daud A, Gonzalez R, Kefford RF, Sosman J, et al. Combined BRAF and MEK inhibition in melanoma with BRAF V600 mutations. N Engl J Med 2012;367:1694–703.
3. Nazarian R, Shi H, Wang Q, Kong X, Koya RC, Lee H, et al. Melanomas acquire resistance to B-RAF(V600E) inhibition by RTK or N-RAS upregulation. Nature 2010;468:973–7.
4. Shi H, Moriceau G, Kong X, Koya RC, Nazarian R, Pupo GM, et al. Preexisting MEK1 exon 3 mutations in V600E/KBRAF melanomas do not confer resistance to BRAF inhibitors. Cancer Discov 2012;2: 414–24.
5. Shi H, Moriceau G, Kong X, Lee MK, Lee H, Koya RC, et al. Melanoma whole-exome sequencing identifies (V600E)B-RAF amplification-mediated acquired B-RAF inhibitor resistance. Nat Commun 2012; 3:724.
6. Long GV, Eroglu Z, Infante J, Patel S, Daud A, Johnson DB, et al. Long-term outcomes in patients with BRAF V600-mutant metastatic melanoma who received dabrafenib combined with trametinib. J Clin Oncol 2018;36:667–73.
7. Hugo W, Shi H, Sun L, Piva M, Song C, Kong X, et al. Non-genomic and immune evolution of melanoma acquiring MAPKi resistance. Cell 2015;162:1271–85.
8. Moriceau G, Hugo W, Hong A, Shi H, Kong X, Yu CC, et al. Tunable-combinatorial mechanisms of acquired resistance limit the efficacy of BRAF/MEK cotargeting but result in melanoma drug addiction. Cancer Cell 2015;27:240–56.
9. Shi H, Hugo W, Kong X, Hong A, Koya RC, Moriceau G, et al. Acquired resistance and clonal evolution in melanoma during BRAF inhibitor therapy. Cancer Discov 2014;4:80–93.
10. Dummer R, Schadendorf D, Ascierto PA, Arance A, Dutriaux C, Di Giacomo AM, et al. Binimetinib versus dacarbazine in patients with advanced NRAS-mutant melanoma (NEMO): a multicentre, open-label, randomised, phase 3 trial. Lancet Oncol 2017;18: 435–45.
11. Hong A, Piva M, Liu S, Hugo W, Lomeli SH, Zoete V, et al. Durable suppression of acquired MEK inhibitor resistance in cancer by sequestering MEK from ERK and promoting antitumor T-cell immunity. Cancer Discov 2021;11:714–35.
12. Cortes-Ciriano I, Lee JJ, Xi R, Jain D, Jung YL, Yang L, et al. Comprehensive analysis of chromothripsis in 2,658 human cancers using whole-genome sequencing. Nat Genet 2020;52:331–41.
13. Song K, Minami JK, Huang A, Dehkordi SR, Lomeli SH, Luebeck J, et al. Plasticity of extrachromosomal and intrachromosomal BRAF amplifications in overcoming targeted therapy dosage challenges. Cancer Discov 2022;12:1046–69.
14. Nathanson DA, Gini B, Mottahedeh J, Visnyei K, Koga T, Gomez G, et al. Targeted therapy resistance mediated by dynamic regulation of extrachromosomal mutant EGFR DNA. Science 2014;343: 72–6.
15. Turner KM, Deshpande V, Beyter D, Koga T, Rusert J, Lee C, et al. Extrachromosomal oncogene amplification drives tumour evolution and genetic heterogeneity. Nature 2017;543:122–5.
16. Helmsauer K, Valieva ME, Ali S, Chamorro Gonzalez R, Schopflin R, Roefzaad C, et al. Enhancer hijacking determines extrachromosomal

circular MYCN amplicon architecture in neuroblastoma. Nat Commun 2020;11:5823.

17. Hung KL, Yost KE, Xie L, Shi Q, Helmsauer K, Luebeck J, et al. ecDNA hubs drive cooperative intermolecular oncogene expression. Nature 2021;600:731–6.

18. Wu S, Bafna V, Mischel PS. Extrachromosomal DNA (ecDNA) in cancer pathogenesis. Curr Opin Genet Dev 2021;66:78–82.

19. Wu S, Turner KM, Nguyen N, Raviram R, Erb M, Santini J, et al. Circular ecDNA promotes accessible chromatin and high oncogene expression. Nature 2019;575:699–703.

20. Shoshani O, Brunner SF, Yaeger R, Ly P, Nechemia-Arbely Y, Kim DH, et al. Chromothripsis drives the evolution of gene amplification in cancer. Nature 2021;591:137–41.

21. Van Allen EM, Wagle N, Sucker A, Treacy DJ, Johannessen CM, Goetz EM, et al. The genetic landscape of clinical resistance to RAF inhibition in metastatic melanoma. Cancer Discov 2014;4:94–109.

22. Hong A, Moriceau G, Sun L, Lomeli S, Piva M, Damoiseaux R, et al. Exploiting drug addiction mechanisms to select against MAPKi-resistant melanoma. Cancer Discov 2018;8:74–93.

23. Chadee DN, Xu D, Hung G, Andalibi A, Lim DJ, Luo Z, et al. Mixed-lineage kinase 3 regulates B-Raf through maintenance of the B-Raf/Raf-1 complex and inhibition by the NF2 tumor suppressor protein. Proc Natl Acad Sci U S A 2006;103:4463–8.

24. Hung KL, Luebeck J, Dehkordi SR, Colon CI, Li R, Wong IT, et al. Targeted profiling of human extrachromosomal DNA by CRISPR-CATCH. Nat Genet 2022;54:1746–54.

25. Morton AR, Dogan-Artun N, Faber ZJ, MacLeod G, Bartels CF, Piazza MS, et al. Functional enhancers shape extrachromosomal oncogene amplifications. Cell 2019;179:1330–41.

26. Zhu Y, Gujar AD, Wong CH, Tjong H, Ngan CY, Gong L, et al. Oncogenic extrachromosomal DNA functions as mobile enhancers to globally amplify chromosomal transcription. Cancer Cell 2021;39: 694–707.

27. Fishilevich S, Nudel R, Rappaport N, Hadar R, Plaschkes I, Iny Stein T, et al. GeneHancer: genome-wide integration of enhancers and target genes in GeneCards. Database (Oxford) 2017;2017:bax028.

28. Rausch T, Jones DT, Zapatka M, Stutz AM, Zichner T, Weischenfeldt J, et al. Genome sequencing of pediatric medulloblastoma links catastrophic DNA rearrangements with TP53 mutations. Cell 2012;148: 59–71.

29. Stephens PJ, Greenman CD, Fu B, Yang F, Bignell GR, Mudie LJ, et al. Massive genomic rearrangement acquired in a single catastrophic event during cancer development. Cell 2011;144:27–40.

30. Zhang CZ, Spektor A, Cornils H, Francis JM, Jackson EK, Liu S, et al. Chromothripsis from DNA damage in micronuclei. Nature 2015;522:179–84.

31. Krupina K, Goginashvili A, Cleveland DW. Causes and consequences of micronuclei. Curr Opin Cell Biol 2021;70:91–9.

32. Alexandrov LB, Kim J, Haradhvala NJ, Huang MN, Tian Ng AW, Wu Y, et al. The repertoire of mutational signatures in human cancer. Nature 2020;578:94–101.

33. Bergstrom EN, Luebeck J, Petljak M, Khandekar A, Barnes M, Zhang T, et al. Mapping clustered mutations in cancer reveals APOBEC3 mutagenesis of ecDNA. Nature 2022;602:510–7.

34. Chang HHY, Pannunzio NR, Adachi N, Lieber MR. Non-homologous DNA end joining and alternative pathways to double-strand break repair. Nat Rev Mol Cell Biol 2017;18:495–506.

35. Korbel JO, Campbell PJ. Criteria for inference of chromothripsis in cancer genomes. Cell 2013;152:1226–36.

36. Maher CA, Wilson RK. Chromothripsis and human disease: piecing together the shattering process. Cell 2012;148:29–32.

37. Dylgjeri E, Knudsen KE. DNA-PKcs: a targetable protumorigenic protein kinase. Cancer Res 2022;82:523–33.

38. Patterson-Fortin J, D'Andrea AD. Exploiting the microhomology-mediated end-joining pathway in cancer therapy. Cancer Res 2020; 80:4593–600.

39. Sharma SV, Lee DY, Li B, Quinlan MP, Takahashi F, Maheswaran S, et al. A chromatin-mediated reversible drug-tolerant state in cancer cell subpopulations. Cell 2010;141:69–80.

40. Song C, Piva M, Sun L, Hong A, Moriceau G, Kong X, et al. Recurrent tumor cell-intrinsic and -extrinsic alterations during MAPKi-induced melanoma regression and early adaptation. Cancer Discov 2017;7:1248–65.

41. Harnor SJ, Brennan A, Cano C. Targeting DNA-dependent protein kinase for cancer therapy. ChemMedChem 2017;12:895–900.

42. Yang C, Tian C, Hoffman TE, Jacobsen NK, Spencer SL. Melanoma subpopulations that rapidly escape MAPK pathway inhibition incur DNA damage and rely on stress signalling. Nat Commun 2021;12:1747.

43. Cowell JK, Miller OJ. Occurrence and evolution of homogeneously staining regions may be due to breakage-fusion-bridge cycles following telomere loss. Chromosoma 1983;88:216–21.

44. Koche RP, Rodriguez-Fos E, Helmsauer K, Burkert M, MacArthur IC, Maag J, et al. Extrachromosomal circular DNA drives oncogenic genome remodeling in neuroblastoma. Nat Genet 2020;52:29–34.

45. Rosswog C, Bartenhagen C, Welte A, Kahlert Y, Hemstedt N, Lorenz W, et al. Chromothripsis followed by circular recombination drives oncogene amplification in human cancer. Nat Genet 2021;53:1673–85.

46. Ly P, Cleveland DW. Rebuilding chromosomes after catastrophe: emerging mechanisms of chromothripsis. Trends Cell Biol 2017;27: 917–30.

47. Ly P, Teitz LS, Kim DH, Shoshani O, Skaletsky H, Fachinetti D, et al. Selective Y centromere inactivation triggers chromosome shattering in micronuclei and repair by non-homologous end joining. Nat Cell Biol 2017;19:68–75.

48. Maciejowski J, Li Y, Bosco N, Campbell PJ, de Lange T. Chromothripsis and kataegis induced by telomere crisis. Cell 2015;163:1641–54.

49. Tang S, Stokasimov E, Cui Y, Pellman D. Breakage of cytoplasmic chromosomes by pathological DNA base excision repair. Nature 2022;606:930–6.

50. Kim H, Nguyen NP, Turner K, Wu S, Gujar AD, Luebeck J, et al. Extrachromosomal DNA is associated with oncogene amplification and poor outcome across multiple cancers. Nat Genet 2020;52:891–7.

51. Labrie M, Brugge JS, Mills GB, Zervantonakis IK. Therapy resistance: opportunities created by adaptive responses to targeted therapies in cancer. Nat Rev Cancer 2022;22:323–39.

52. Hammarsten O, DeFazio LG, Chu G. Activation of DNA-dependent protein kinase by single-stranded DNA ends. J Biol Chem 2000;275: 1541–50.

53. Li H, Durbin R. Fast and accurate short read alignment with Burrows-Wheeler transform. Bioinformatics 2009;25:1754–60.

54. Li H, Handsaker B, Wysoker A, Fennell T, Ruan J, Homer N, et al. The sequence alignment/map format and SAMtools. Bioinformatics 2009;25:2078–9.

55. Talevich E, Shain AH, Botton T, BBC CNVkit.: Genome-wide copy number detection and visualization from targeted DNA sequencing. PLoS Comput Biol 2016;12:e1004873.

56. Miller CA, Hampton O, Coarfa C, Milosavljevic A. ReadDepth: a parallel R package for detecting copy number alterations from short sequencing reads. PLoS One 2011;6:e16327.

57. Wala JA, Bandopadhayay P, Greenwald NF, O'Rourke R, Sharpe T, Stewart C, et al. SvABA: genome-wide detection of structural variants and indels by local assembly. Genome Res 2018;28:581–91.

58. Eisfeldt J, Vezzi F, Olason P, Nilsson D, Lindstrand A. TIDDIT, an efficient and comprehensive structural variant caller for massive parallel sequencing data. F1000Res 2017;6:664.

59. Rausch T, Zichner T, Schlattl A, Stutz AM, Benes V, Korbel JO. DELLY: structural variant discovery by integrated paired-end and split-read analysis. Bioinformatics 2012;28:i333–i9.

60. Deshpande V, Luebeck J, Nguyen ND, Bakhtiari M, Turner KM, Schwab R, et al. Exploring the landscape of focal amplifications in cancer using AmpliconArchitect. Nat Commun 2019;10:392.

61. Kim S, Scheffler K, Halpern AL, Bekritsky MA, Noh E, Kallberg M, et al. Strelka2: fast and accurate calling of germline and somatic variants. Nat Methods 2018;15:591–4.

62. Blokzijl F, Janssen R, van Boxtel R, Cuppen E. MutationalPatterns: comprehensive genome-wide analysis of mutational processes. Genome Med 2018;10:33.

63. Khan A, Zhang X. dbSUPER: a database of super-enhancers in mouse and human genome. Nucleic Acids Res 2016;44:D164–71.

64. Dobin A, Davis CA, Schlesinger F, Drenkow J, Zaleski C, Jha S, et al. STAR: ultrafast universal RNA-seq aligner. Bioinformatics 2013;29:15–21.

65. Liao Y, Smyth GK, Shi W. featureCounts: an efficient general purpose program for assigning sequence reads to genomic features. Bioinformatics 2014;30:923–30.

66. Robinson MD, Oshlack A. A scaling normalization method for differential expression analysis of RNA-seq data. Genome Biol 2010;11:R25.

67. Shi H, Hong A, Kong X, Koya RC, Song C, Moriceau G, et al. A Novel AKT1 mutant amplifies an adaptive melanoma response to BRAF inhibition. Cancer Discov 2014;4:69–79.